# Quantification and evaluation of atmospheric pollutant emissions from open biomass burning with multiple methods: A case study for Yangtze River Delta region, China

Yang Yang[1] and Yu Zhao[1,2*]

1. State Key Laboratory of Pollution Control & Resource Reuse and School of the Environment, Nanjing University, 163 Xianlin Ave., Nanjing, Jiangsu 210023, China

2. Jiangsu Collaborative Innovation Center of Atmospheric Environment and Equipment Technology (CICAEET), Nanjing University of Information Science & Technology, Jiangsu 210044, China

*Corresponding author: Yu Zhao

Phone: 86-25-89680650; email: yuzhao@nju.edu.cn

## Abstract

Air pollutant emissions from open biomass burning (OBB) in Yangtze River Delta (YRD) were estimated for 2005-2015 using three (traditional bottom-up, fire radiative power (FRP)-based, and constraining) approaches, and the differences between those methods and their sources were analyzed. The species included $PM_{10}$, $PM_{2.5}$, organic carbon (OC), elemental carbon (EC), $CH_4$, non-methane volatile organic compounds (NMVOCs), CO, $CO_2$, $NO_X$, $SO_2$ and $NH_3$. The inter-annual trends in emissions with FRP-based and constraining methods were similar with the fire counts in 2005-2012, while that with traditional method was not. For most years, emissions of all species estimated with constraining method were smaller than those with traditional method except for NMVOCs, while they were larger than those with FRP-based except for EC, $CH_4$ and $NH_3$. Such discrepancies result mainly from different masses of crop residues burned in the field (CRBF) estimated in the three methods. Chemistry transport modeling (CTM) was applied using the three OBB inventories. The simulated $PM_{10}$ concentrations with constrained emissions were closest to available observations, implying constraining method provided the best emission estimates. CO emissions in the three methods were compared with other studies. Similar temporal variations were found for the constrained emissions, FRP-based emissions, GFASv1.0 and GFEDv4.1s, with the largest and the lowest emissions estimated for 2012 and 2006, respectively. The temporal variations of the emissions based on traditional method, GFEDv3.0 and Xia et al. (2016) were different with them. The constrained CO emissions in this study were commonly smaller than those based on traditional bottom-up method and larger than those based on burned area or FRP in other studies. In particular, the constrained emissions were close to GFEDv4.1s that contained emissions from small fires. The contributions of OBB to two particulate pollution events in 2010 and 2012 were analyzed with brute-force method. Attributed to varied OBB emissions and meteorology, the average contribution of OBB to $PM_{10}$ concentrations in June 8-14 2012 was estimated at 37.6% (56.7 $\mu g/m^3$), larger than that in June 17-24, 2010 at 21.8 % (24.0 $\mu g/m^3$). Influences of diurnal curves of OBB emissions and meteorology on air pollution caused by OBB were evaluated by designing simulation scenarios, and the results suggested that air pollution caused by OBB would become heavier if the meteorological conditions were unfavorable, and that more attention should be paid to

the OBB control at night. Quantified with Monte-Carlo simulation, the uncertainty of traditional bottom-up inventory was smaller than that of FRP-based one. The percentages of CRBF and emission factors were the main source of uncertainty for the two approaches, respectively. Further improvement on CTM for OBB events would help better constraining OBB emissions.

## 1. Introduction

Open biomass burning (OBB) is an important source of atmospheric particulate matter (PM) and trace gases including methane ($CH_4$), non-methane volatile organic compounds (NMVOCs), carbon monoxide (CO), carbon dioxide ($CO_2$), oxides of nitrogen ($NO_X$), sulfur dioxide ($SO_2$), and ammonia ($NH_3$) (Andreae and Merlet, 2001; van der Werf et al., 2010; Wiedinmyer et al., 2011; Kaiser et al., 2012; Giglio et al., 2013, Qiu et al., 2016; Zhou et al., 2017a). As it has significant impacts on air quality and climate (Crutzen and Andreae, 1990; Cheng et al., 2014; Hodzic and Duvel, 2018), it is important to understand the amount, temporal variation and spatial pattern of OBB emissions.

Various methods have been used to estimate OBB emissions, including traditional bottom-up method that relied on surveyed amount of biomass burning (traditional bottom-up method), the method based on burned area or fire radiative power (BA or FRP method), and emission constraining with chemistry transport model (CTM) and observation (constraining method). In the traditional bottom-up method that was most frequently used, emissions were calculated as a product of crop production level, the ratio of straw to grain, percentage of dry matter burned in fields, combustion efficiency, and emission factor (Streets et al., 2003; Cao et al., 2007; Wang and Zhang, 2008; Zhao et al., 2012; Xia et al., 2016, Zhou et al., 2017a). The BA or FRP method was developed along with progress of satellite observation technology. BA was detected through remote sensing, and used in OBB emission calculation combined with ground biomass density burned in fields, combustion efficiency and emission factor. As burned area of each agricultural fire was usually small and difficult to be detected, this method could seriously underestimate the emissions (van der Werf et al., 2010; Liu et al., 2015). In FRP-based method, fire radiative energy (FRE) was calculated with FRP at over pass time of satellite and the diurnal cycle of FRP. The mass of crop residues burned in the field (CRBF) were then

obtained based on combustion conversion ratio and FRE, and emissions were calculated as a product of the mass of CRBF and emission factor (Kaiser et al., 2012; Liu et al., 2015). In the constraining method, observed concentrations of atmospheric compositions were used to constrain OBB emissions with CTM (Hooghiemstra et al., 2012; Krol et al., 2013; Konovalov et al., 2014). The spatial and temporal distributions of OBB emissions were derived from information of fire points from satellite observation. Although varied methods and data sources might lead to discrepancies in OBB emission estimation, those discrepancies and underlying reasons have seldom been thoroughly analyzed in previous studies. Moreover, few studies applied CTM to evaluate emissions obtained from different methods, thus the uncertainty and reliability in OBB emission estimates remained unclear.

Due to growth of economy and farmers' income, a large number of crop straws were discharged and burned in field, and OBB (which refers to crop straws burned in fields in this paper) became an important source of air pollutants in China (Streets et al., 2003; Shi and Yamaguchi 2014; Qiu et al., 2016; Zhou et al., 2017a). It brings additional pressure to the country, which is suffering poor air quality (Richter et al., 2005; van Donkelaar et al., 2010; Xing et al., 2015; Guo et al., 2017) and making efforts to reduce pollution (Xia et al., 2016; Zheng et al., 2017). Located in the eastern China, Yangtze River Delta (YRD) including the city of Shanghai and the provinces of Anhui, Jiangsu and Zhejiang is one of China’s most developed and heavy-polluted regions (Ran et al., 2009; Xiao et al., 2011; Cheng et al., 2013, Guo et al., 2017). Besides intensive industry and fossil fuel combustion, YRD is also an important area of agriculture production, and frequent OBB events aggravated air pollution in the region (Cheng et al., 2014).

In this study, we chose YRD to develop and evaluate high resolution emission inventories of OBB with different methods. Firstly, we established YRD’s OBB emission inventories for 2005-2012 using the traditional bottom-up method (the percentages of CRBF for 2013-2015 were currently unavailable), and inventories for 2005-2015 using FRP-based and constraining methods. The three inventories were then compared with each other and other available studies, in order to discover the differences and their origins. Meanwhile, the three inventories were evaluated using Models-3 Community Multi-scale Air Quality (CMAQ) system and available ground observations. Contributions of OBB to particulate pollution during three typical OBB events in 2010, 2012 and 2014 were evaluated through brute-force method. Influences

of meteorology and diurnal curves of OBB emissions on air pollution caused by OBB were also analyzed by designing simulation scenarios. Finally, uncertainties of the three OBB inventories were analyzed and quantified with Monte-Carlo simulation.

## 2. Data and methods

### 2.1 Traditional bottom-up method

Annual OBB emissions in YRD were calculated by city from 2005 to 2012 using the traditional bottom-up method with following equations:

$$E_{(i,y),j} = \sum_{k} \left( M_{(i,y),k} \times EF_{j,k} \right) \quad (1)$$

$$M_{(i,y),k} = P_{(i,y),k} \times R_k \times F_{(i,y)} \times CE_k \quad (2)$$

where $i$ and y indicate city and year (2005-2012), respectively; $j$ and $k$ represent species and crop type, respectively; $E$ is the emissions, metric ton (t); $M$ is the mass of CRBF, Gg; $EF$ is the emission factor, g/kg; $P$ is the crop production, Gg; $R$ is the ratio of grain to straw (dry matter); $F$ is the percentage of CRBF; and $CE$ is the combustion efficiency.

As summarized in Table S1 in the supplement, emission factors were obtained based on a comprehensive literature review, and those developed in China were selected preferentially. The mean value was used if various emission factors could be obtained. When the emission factors for one crop straw were not obtained, the mean value of the others was used instead. Annual production of crops at city level was taken from statistical yearbooks (NBS, 2013). The ratios of straw to grain for different crops were obtained from Bi (2010) and Zhang et al. (2008), and the combustion efficiencies for different crop were obtained from Wang et al. (2013), as provided in Table S2 in the supplement. Without officially reported data, the percentages of CRBF were estimated to be half of the percentages of unused crop residues, following Su et al. (2012). In Jiangsu, the percentages of unused crop residues were officially reported for 2008, 2011 and 2012, while data for other years were unavailable. In this work, therefore, the percentages of CRBF were assumed to be constant before 2008 and to decrease by same rate (-15.2%) from 2008 to 2011, since a provincial plan was made in 2009 to increase the utilization of straw (JPDRC and SMAC, 2009). Similarly, the percentages of CRBF for Shanghai were assumed to be constant before 2008 and to decrease by same rate (-16.8%) from 2008 to 2012. Without any official plans

150 released, in contrast, constant percentages of CRBF were assumed for Zhejiang and
151 Anhui before 2011, and that for 2012 was taken from NDRC (2014). We applied
152 uniform percentages of CRBF for cities within a province attributed to lack of detailed
153 information at city level, as summarized in Table S3 in the supplement. OBB
154 emissions after 2012 were not calculated with the traditional bottom-up method,
155 attributed to lack of information on percentages of CRBF and unused crop residues
156 for corresponding years.

157 **2.2 FRP-based method**

158 Similar to traditional bottom-up method, OBB emissions of FRP-based method
159 were calculated by multiplying the mass of CRBF and emission factors of various
160 pollutants, but mass of CRBF were derived from FRP instead of government-reported
161 data. As the burned crop types could not be identified with FRP, uniform emission
162 factors were applied for different crop types (Randerson et al., 2018; Liu et al., 2016;
163 Qiu et al., 2016), as provided in Table S4 in the supplement.

164 The mass of CRBF was calculated with the following equation:

165 $$M = FRE \times CR \tag{3}$$

166 where *M* represents the mass of CRBF, kg; *CR* represents the combustion conversion
167 ratio from energy to mass (kg/MJ); and *FRE* represents the total released radiative
168 energy in an active fire pixel obtained from satellite observation (MJ). We used a
169 combustion ratio (*CR*) of 0.41 $\pm$ 0.04 (kg/MJ) based on the results of Wooster et al.
170 (2005) in the field and Freeborn et al. (2008) in the laboratory. Diurnal cycle of FRP
171 from crop burning was assumed to follow a Gaussian distribution. Following Vermote
172 et al. (2009) and Liu et al. (2015), *FRE* was calculated using a modified Gaussian
173 function as below:

174 $$FRE = \int FRP = \int_0^{24} FRP_{\text{peak}} \left( \text{b} + \text{e}^{-\frac{(t-h)^2}{2\sigma^2}} \right) dt \tag{4}$$

175 $$FRP_{\text{peak}} = \frac{FRP_t}{\left[ \text{b} + \text{e}^{-\frac{(t-h)^2}{2\sigma^2}} \right]} \tag{5}$$

176 where $FRP_{peak}$ is the peak fire radiative power in the fire diurnal cycle; *t* is the
177 overpass time of satellite; and *b*, $\sigma$, and *h* represent the background level of the diurnal
178 cycle, the width of fire diurnal curve, and the peak hour (local time, LT), respectively.

179 FRP data were taken from MODIS Global Monthly Fire Location Product
180 (MCD14ML) which provides data from both the Terra and Aqua satellites (Davies et

al., 2009). The active fire data in MCD14ML were derived from Terra with overpass times at approximately 10:30 AM and 10:30 PM LT and Aqua satellite with overpass times at 1:30 AM and 1:30 PM LT. The fire products provided the geographic coordinates of fire pixels (also known as fire points), overpass times, satellites and their FRP values. The land cover dataset (GlobCover2009) was used to define croplands (European Space Agency and Université Catholique de Louvain, 2011).

Parameters $b$, $\sigma$, and $h$ from 2005 to 2015 were calculated using the inter-annual Terra to Aqua (T/A) FRP ratios provided in Table S5 in the supplement:

$$b = 0.86r^2 - 0.52r + 0.08 \quad (6)$$

$$\sigma = 3.89r + 1.03 \quad (7)$$

$$h = -1.23r + 14.57 + \varepsilon \quad (8)$$

where $r$ represents the average T/A FRP ratio. Following Liu et al. (2015), we added a parameter $\varepsilon$ (4h) to modify $FRP_{peak}$ hour (h) of the diurnal curve, and the modified FRP diurnal curves could better represent observed FRP temporal variability than the original, as shown in Figure S1 in the supplement. As a result, FRE was calculated to range from $1.49\times10^6$ MJ in 2009 to $1.95\times10^6$ MJ in 2005, with a mean value of $1.74\times10^6$ MJ for YRD region (Table S5).

To further understand the sources of discrepancies between bottom-up and FRP-based methods, the emission factors applied in the bottom-up method were weighted with the masses of various crop types and used to estimate the OBB emissions for 2010 with the FRP-based method. The estimated OBB emissions (FRP-based (WSE)) were compared with the emissions based on bottom-up method in section 3.3.

### 2.3 Constraining method

CTM and observation of ground particle matter (PM) concentrations were applied in constraining OBB emissions given the potentially big contribution of OBB to particle pollution for harvest seasons (Fu et al., 2013; Cheng et al., 2014; Li et al., 2014). To characterize the non-linearity between emissions and concentrations, an initial inventory including OBB and other sources was applied in CTM, and the response of PM concentrations to emissions was calculated by changing OBB emissions by a certain fraction (5% in this study) in the model. We defined a response coefficient as the ratio of relative change in PM concentrations to that in OBB

emissions. Simulated PM concentrations were then compared with available observation, and the mass of CRBF and OBB emissions of all species were corrected combining the obtained response coefficient and the discrepancy between observed and simulated PM concentrations. The corrected emissions were further applied in CTM and the process (including recalculation of response coefficient) repeated until the discrepancies between observation and simulation was small enough (the value of I in equation (9) is less than 0.1% in this study). To limit the potential uncertainty in emissions from other sources, the differences between simulated and observed PM concentrations for non-OBB event period were included in the analysis:

$$I = \left| \frac{\sum_{x,i} S_{x,i} - \sum_{x,i} Q_{x,i} \times N_i}{\sum_{x,i} O_{x,i}} - 1 \right| \quad (9)$$

where $x$ and $i$ stand for the time (time interval of simulation is hour) and city, respectively; $O$ is the observed PM concentration; $S$ and $Q$ are the simulated PM concentration with and without OBB emissions, respectively; and $N$ is the normalized mean bias (NMB) for non-OBB event period. The constraining method did not rely on the activity levels (i.e., the burned biomass in the cropland) that were still of considerable uncertainty in China. The estimation in emissions of the species for which the ground observation was applied as constraint ($PM_{10}$ in this case) was less influenced by the uncertainties of emission factors compared to the other two methods.

As primary particles emitted from OBB are almost fine ones, ambient $PM_{2.5}$ concentrations were commonly observed to account for large fractions of $PM_{10}$ during the OBB event. Figure S2 shows the observed concentrations of $PM_{2.5}$ and $PM_{10}$ at Caochangmen station in Nanjing (the capital of Jiangsu) in June 2012, and the average mass ratio of $PM_{2.5}$ to $PM_{10}$ reached 79% during the OBB event in June 8-14, 2012. The ratios might be even higher in northern YRD where most fire points were detected. As ground $PM_{2.5}$ concentrations were unavailable in most cities of northern YRD before 2013, we expected that $PM_{10}$ was an appropriate indicator for OBB pollution, and observed $PM_{10}$ concentrations were used to constrain OBB emissions instead in this study. The daily mean $PM_{10}$ concentrations of all cities were derived from the officially reported Air Pollution Index (API) by China National

Environmental Monitoring Center (http://www.cnemc.cn/). The conversion from API scores to $PM_{10}$ concentrations is discussed in the Supplement.

Figure 1 illustrated the spatial patterns of fire points (panels a1 and a2) in June 2010 and 2012, city-level $PM_{10}$ concentrations in YRD region in June 2010 and 2012 (panels b1 and b2), and temporal variations of daily fire occurrences in June 2010 and 2012 (panels c1 and c2). From 2005 to 2012, most OBB activities were found in June 2010 and 2012 and northern YRD was the region with the intensive fire counts. Accordingly $PM_{10}$ concentrations in northern YRD cities were higher than those in more developed and industrialized cities in the eastern YRD (e.g., Shanghai, Suzhou, Wuxi, and Changzhou), because emissions of OBB overwhelmed those from other sources (Li et al., 2014; Huang et al., 2016). Therefore we constrained OBB emissions with observed $PM_{10}$ concentrations in northern YRD cities including Xuzhou, Lianyungang, Fuyang, Bengbu, Huainan, Hefei, Chuzhou and Bozhou. Suggested by the monthly and daily distribution of fire counts (Figures S3 and 1c), two strong OBB events were defined for June 17-24, 2010 and June 8-14, 2012, and other days in June of 2010 and 2012 were defined as non-OBB event period. For other years, OBB emissions were first scaled from the constrained emissions in 2010 and 2012 with the ratios of FRE for corresponding year to that for 2010 and 2012 respectively, and then calculated as average of the two. Remarkably, the correction of activity level was based on the comparisons of simulated and observed $PM_{10}$ concentrations, and the emissions of other species were revised according to the changed activity level. The reliability of emission estimation for other species thus depended largely on the reliability of emission factors for $PM_{10}$ and those species. Uncertainty would be introduced to the method, attributed to lack of sufficient and qualified domestic measurements on emission factors.

Traditional bottom-up method was used to calculate the initial emission input for all species (NMVOCs emission factor was taken from FRP-based method instead as those in bottom-up method (Li et al., 2007) did not contain oxygenated VOCs). In contrast to application of uniform percentage of CRBF within one province, however, percentage of CRBF for each city was calculated based on that in whole YRD and the fraction of FRP in the city to total YRD FRP, to make the spatial distribution of OBB emissions consistent with that of FRP all over YRD region:

$$F_{(i,y)} = \frac{FRP_{(i,y)}}{FRP_{(YRD,y)}} \times \frac{\sum_k P_{(YRD,y),k}}{\sum_k P_{(i,y),k}} \times F_{(YRD,y)} \quad (10)$$

where *i* and *k* represent city and crop type, respectively; *y* indicates the year (2010 and 2012); *F*, *P*, and *FRP* are the percentage of CRBF, crop production, and fire radiative power, respectively. The initial percentage of CRBF for total YRD ($F_{(YRD,y)}$ in eq (10)) was expected to have limited impact on the result and it was set at 10%, smaller than those in previous studies (Streets et al., 2003; Cao et al., 2007; Wang and Zhang, 2008; Zhao et al., 2012; Xia et al., 2016, Zhou et al., 2017a).

## 2.4 Temporal and spatial distributions

The spatial and temporal patterns of OBB emissions in the three inventories were determined according to the FRP of agricultural fire points. The emissions of *m*-th grid in region *u* on *n*-th day in year *y* were calculated using equation (11):

$$E_{(m,n),j} = \frac{FRP_{(m,n)}}{FRP_{(u,y)}} \times E_{(u,y),j} \quad (11)$$

where $FRP_{(m,n)}$ is the FRP of *m*-th grid on *n*-th day; $FRP_{(u,y)}$ and $E_{(u,y),j}$ are the total FRP and OBB emissions of species *j* for region *u* in year y, respectively. The region *u* indicates city for FRP-based and constraining method, while it indicates province for traditional bottom-up method since uniform percentages of CRBF was applied within the same province in the method.

## 2.5 Configuration of air quality modeling

The Models-3 Community Multi-scale Air Quality (CMAQ) version 4.7.1 was applied to constrain OBB emissions and to evaluate OBB inventories with different methods. As shown in Figure 2, one-way nested domain modeling was conducted, and the spatial resolutions of the two domains were set at 27 and 9 km respectively in Lambert Conformal Conic projection, centered at (110$^o$E, 34$^o$N) with two true latitudes 25 and 40° N. The mother domain (D1, 180×130 cells) covered most parts of China, Japan, North and South Korea, while the second domain (D2, 118×97 cells) covered the whole YRD region. OBB inventories developed in this work were applied in D2. Emissions from other anthropogenic sources in D1 and D2 were obtained from the downscaled the Multi resolution Emission Inventory for China (MEIC, http://www.meicmodel.org/) with an original spatial resolution of 0.25°×0.25°. Population density was applied to relocate MEIC to each modeling domain. Biogenic

emission inventory was from the Model Emissions of Gases and Aerosols from Nature developed under the Monitoring Atmospheric Composition and Climate project (MEGAN MACC, Sindelarova et al., 2014), and the emission inventories of Cl, HCl and lightning $NO_X$ were from the Global Emissions Initiative (GEIA, Price et al., 1997). Meteorological fields were provided by the Weather Research and Forecasting Model (WRF) version 3.4, and the carbon bond gas-phase mechanism (CB05) and AERO5 aerosol module were adopted. Other details on model configuration and parameters were given in Zhou et al. (2017b).

Meteorological parameters of WRF model were compared with the observation dataset of US National Climate Data Center (NCDC), as summarized in Table S6 in the Supplement. For June 2010, the average biases between the two datasets were 0.06 m/s for wind speed, 9.84 degree for wind direction, 0.64 K for temperature and 2.99% for relative humidity. The analogue numbers were 0.01 and 0.67 m/s, 7 and 18.22 degree, 0.91 and 0.43 K and 3.1 and 0.07% respectively for June 2012 and 2014, respectively. The meteorological parameters of this study were in compliance with the benchmarks derived from Emery et al. (2001) and Jiménez et al. (2006). Simulated daily $PM_{10}$ concentrations were compared with observation for non-OBB event period in June 2010 and 2012 in Table S7 in the supplement. The average of normalized mean biases (NMB) and normalized mean errors (NME) were -19.2% and 38.9% for 17 YRD cities in June 2010, and -20.9% and 33.9% for 22 cities in June 2012, respectively. Simulated daily and hourly $PM_{2.5}$, $PM_{10}$ and CO concentrations were compared with the observation for non-OBB event period in June 2014 in Table S8 and S9 in the supplement. The hourly NMB of $PM_{2.5}$ and $PM_{10}$ were -29.9% and -39.8%, and the hourly NME of $PM_{2.5}$ and $PM_{10}$ were 49.8% and 54.7%. The model performance of $PM_{2.5}$ and $PM_{10}$ was similar with that derived by Zhang et al. (2006) in US in general. The hourly NMB and NME of CO were -42.3% and 48.3%, and they were similar with those derived by Kota et al. (2018). As shown in Figure S4 in the supplement, moreover, simulated hourly $PM_{10}$ and $PM_{2.5}$ concentrations were in good agreement with observations at four air quality monitoring sites in YRD during non-OBB event period in June 2012. The comparison thus implied the reliability of emission inventory of anthropogenic origin used in this work, while underestimation might occur indicated by the negative NMB.

## 3. Results and discussions

### 3.1 OBB emissions estimated with the three methods

OBB emissions estimated with the traditional bottom-up method for 2005-2012 were shown in Table S10 in the supplement. As emission factors were assumed unchanged during the period, similar inter-annual trends were found for all species and $CO_2$ was selected as a representative species for further discussion. As shown in Figure 3, $CO_2$ emissions from traditional bottom-up method were estimated to decrease from 23000 in 2005 to 19973 Gg in 2012, with a peak value of 27061 Gg in 2008. In contrast, the number of fire points in YRD farmland increased from 7158 in 2005 to 17074 in 2012. The fire counts detected from satellite thus did not support the effectiveness of OBB restriction by government in YRD before 2013. Table S11 in the supplement presents the annual OBB emissions derived from FRP-based method for 2005-2015 in YRD region. Associated with fire counts, $CO_2$ emissions were estimated to grow by 119.7% from 2005 to 2012, with the largest and the second largest annual emissions calculated at 19977 and 12718 Gg for 2012 and 2010, respectively (Figure 3). Similar temporal variability was found for fire counts, which increased by 138.5% from 2005 to 2012, with the most and the second most counts found at 17074 and 12322 for 2012 and 2010, respectively.

With the constraining method, as shown in Figure S5 in the supplement, the ratio of constrained mass of CRBF for 2012 to 2010 was 1.51, clearly lower than the ratios of original FRE (1.75) but close to the ratio of modified FRE for 2012 to 2010 (1.57). The comparison suggested that modified FRE better reflect the OBB activity in YRD than original FRE. In order to make the ratio of FRE for the two years be closer to the ratio of constrained mass of CRBF, an improved method was developed for calculating the FRE. Given the possible variation of $FRP_{peak}$ hour between years, we obtained the diurnal cycle of total FRP of YRD for 2005-2015 based on Gaussian fitting as shown in Figure S6 in the supplement. The ratio of FRE for 2012 to 2010 was recalculated at 1.54, further closer to the ratio of constrained mass of CRBF. Therefore the ratios of FRE for another given year to 2012 and 2010 were calculated with this improved method, and were then applied to emission scaling for that year. The constrained OBB emissions from 2005 to 2015 were summarized in Table 1. The inter-annual trend in constrained emissions was similar with those in fire counts and FRP-based emissions but different from that in emissions with traditional bottom-up

method, as shown in Figure 3. It is usually difficult to collect accurate percentages of CRBF from bottom-up method, as it demands intensive investigation in the rural areas. In addition, the percentages of CRBF were not updated for each year, and same percentages were commonly applied for years without sufficient data support from local surveys.

The constrained $CO_2$ emissions for Jiangsu, Anhui, Zhejiang and Shanghai were calculated at 5790, 4699, 1104 and 419 Gg in 2005, accounting for 48.2%, 39.1%, 9.2% and 3.5% of total OBB emissions in YRD, respectively. The analogue numbers for 2012 were 7345, 16159, 2574 and 394 Gg, and 27.7%, 61.0%, 9.7% and 1.5%, respectively. Jiangsu and Anhui were found to contribute largest to OBB emissions in YRD for 2005 and 2012, respectively. In the traditional bottom-up method, however, Anhui was estimated to contribute largest for both years. City-level OBB emissions estimated with the three methods were summarized in Table S12-S14 in the supplement. With the constraining method, in particular, largest $CO_2$ emissions were found in Suzhou (1708 Gg) of Anhui, Lianyungang (1578 Gg) and Xuzhou (1401 Gg) of Jiangsu in 2005, accounting for 14.2%, 13.1% and 11.7% of the total emissions, respectively. In 2012, Suzhou, Bozhou of Anhui, and Xuzhou of Jiangsu were identified as the cities with the largest emissions, with the values estimated at 5007, 2433, and 2109 Gg, respectively. Depending on distribution of fire points, the shares of OBB emissions by city were close between constraining and FRP-based method, and large emissions concentrated in the north of YRD. Based on surveyed percentages of CRBF and crop production, in contrast, the emission shares by city in traditional bottom-up method were clearly different from the other two, and emissions concentrated in Anhui cities with high crop production level.

The average annual emissions of $CO_2$ for 2005-2011 with traditional bottom-up method were 87.0% larger than those in constraining method and the emissions for 2012 was 24.6% times smaller than those in constraining method. Given the same sources of emission factors for all species except NMVOCs, the discrepancies of OBB emissions for most species between constraining and traditional bottom-up methods come from the activity levels (i.e., percentages of CRBF and crop production). The average annual constrained emissions from 2005 to 2015 were larger than those derived by FRP-based method for all species except EC, $CH_4$ and $NH_3$, since the average annual mass of CRBF from constraining method were 36.9% larger than those from FRP-based method for these years, as shown in Figure S7.

The percentage of CRBF is an important parameter to judge OBB activity and to estimate emissions. Besides the investigated values applied in traditional bottom-up approach, the percentages of CRBF were recalculated based on the constrained emissions at provincial level and were shown in Figure S8 in the supplement. The largest and smallest percentages of CRBF in the whole YRD region were estimated at 18.3% in 2012 and 8.1% in 2006, respectively. The inter-annual trend in percentages of CRBF for YRD was closest to that for Anhui province, as the province dominated the crop burning in the region. The different inter-annual trends by province were strongly influenced by agricultural practice and government management. Agricultural practice could be associated with income level and mechanization level. Increased income, would lead to more crop residues discarded and burned in the field, while development of mechanization would lead to less. The constrained percentages of CRBF for Shanghai increased from 2005 to 2007 and declined after 2007, while those for Jiangsu decreased from 2005 to 2008 and increased after 2008. Increasing trends were found for the percentages of CRBF for Anhui and Zhejiang from 2005 to 2012, and they might result largely from growth of farmers' income. Note that percentages of CRBF for all provinces except Zhejiang decreased significantly in 2008, attributed largely to the measures of air quality improvement for Beijing Olympic Games. Shanghai was the only one with its percentage of CRBF significantly reduced in 2010, resulting mainly from the air pollution control for Shanghai World Expo in that year. Compare to the percentages of CRBF used in bottom-up method, the constrained ones of Anhui and Jiangsu for all the years except 2012 were smaller, leading to lower constrained OBB emissions than bottom-up ones in those years.

The constrained percentages of CRBF and straw yields for 2012 were shown by city in Figure S9 in the supplement, and clear inconsistency in spatial distributions can be found. The percentage of CRBF was not necessarily high for a city with large straw production. For instance, straw production of Yancheng was higher than most other cities, but its percentage of CRBF was 5.7% and lower than most other cities. Through linear regression, correlation coefficient was calculated at only 0.06 between constrained percentage of CRBF and straw yield at city level. The poor correlation between them thus suggested that large uncertainty could be derived if uniform percentage of CRBF was applied to calculate OBB emissions for cities within given province, as what we did in the traditional bottom-up methodology.

### 3.2 Evaluation of the three OBB inventories with CMAQ

Figures 4 and 5 illustrate the observed 24-hour averaged and simulated hourly $PM_{10}$ concentrations for selected YRD cities in June 17-25, 2010 and June 8-14, 2012, respectively. Four emission cases, i.e., inventory without and with OBB emissions estimated using the three methods, were included. The simulated $PM_{10}$ concentrations without OBB emissions were significantly lower than observation for all cities, implying that OBB was an important source of airborne particulates during the two periods. Simulations with OBB emissions derived from the three methods performed better than those without OBB emissions for most cities during June17-25, 2010 and all cities during June 8-14, 2012. The best performance was found for simulations with constrained OBB emissions in most cities during the two periods, and the high $PM_{10}$ concentrations were generally caught by CTM for the concerned OBB events. In 2010, the observed high concentrations were simulated with constrained emissions in Lianyungang during June 21-23, and Fuyang and Huainan during June 19-21. In 2012, the observed high concentrations were caught with constrained emissions in Xuzhou during June 12-14, Lianyungang during June 13-14, Fuyang during June 11-12, Bozhou during June 10 and Chuzhou during June 11-12. The results thus indicated that fire points could principally capture the temporal and spatial distribution of OBB emissions. Overestimation still existed with constrained OBB emissions for the cities with intensive fire points (e.g., Xuzhou, Bozhou and Fuyang in 2012 and Bengbu in 2010), while underestimation commonly existed for cities with fewer fire points (e.g., Hefei, Chuzhou and Huainan in 2010 and 2012). Due to limitation of MODIS observation, fires at moderate to small scales could not be fully detected (Giglio et al., 2003; Schroeder et al., 2008), thus the spatial allocation of OBB emissions based on FRP could possibly result in more emissions than actual in areas with intensive fire points. Moreover, we used $PM_{2.5}$, $PM_{10}$ and CO concentrations (which were available since 2013) to evaluate the model performances when the constrained, FRP-based or no OBB emissions were applied in CTM for an OBB event during June 7-13, 2014. Figures S10 and S11 in the supplement illustrate the observed and simulated hourly concentrations for $PM_{2.5}$ and $PM_{10}$ in selected YRD cities, respectively. The best performance was found for simulations with the constrained OBB emissions in most cities during the period, and the peak particle concentrations were generally caught by CTM. The observed high concentrations were simulated with the constrained emissions in Lianyungang and Suqian on June 12 and Huaian and Yancheng on June

13. Figures S12 in the supplement illustrates the observed and simulated hourly concentrations for CO in selected YRD cities, respectively. The best performance was found for simulations with the constrained OBB emissions in most cities during the period, and the observed high CO concentrations were simulated with the constrained emissions in Xuzhou and Huaian on June 13.

The NMB and NME between observed and simulated $PM_{2.5}$ and $PM_{10}$ concentrations are shown in Table 2. In most cases, the NMB and NME with constrained OBB emissions were smaller than those with other OBB emissions, implying the best guess of OBB emissions obtained through the constraining method combining CTM and ground observation. The simulated $PM_{2.5}$ and $PM_{10}$ concentrations using FRP-based OBB emissions were smaller than observation for the three periods, due mainly to the mass of CRBF were underestimated. The results thus indicated that OBB emissions might be underestimated in FRP-based method in 2010, 2012 and 2014, since many small fires in YRD were undetected in MODIS active fire detection products. The probability of MODIS detection was strongly dependent upon the temperature and area of the fire being observed. The average probability of detection for tropical savanna was 33.6% when the temperature of fire was between 600 and 800 ℃ and the area of fire was between 100 and 1000 $m^2$ (Giglio et al., 2003). In YRD region, on one hand, the fire temperature of crop residue burned in fields was relatively low. On the other hand, nearly 100 farmers were possibly located in a single $1\times1$ km MODIS pixel (Liu et al., 2015), and a famer commonly owned croplands of several hundred square meters. Therefore many fire pixels in YRD might not be detected, leading to underestimation in the total FRE. The simulated $PM_{10}$ concentrations using traditional bottom-up OBB emissions were higher than observation in 2010 but lower in 2012. The results thus implied the growth in OBB emissions from 2010 to 2012 could not be captured by traditional bottom-up method, attributed partly to application of unreliable percentage of CRBF. We further selected the performance of CMAQ modeling in US (Zhang et al., 2006) as the benchmark for $PM_{2.5}$ and $PM_{10}$ simulation. As can be seen in Table 2, the NMBs and NMEs for most case with the constrained OBB emissions were close to those by Zhang et al. (2006). The NMEs for hourly $PM_{2.5}$ and $PM_{10}$ were slightly larger. Given the larger uncertainty in emission inventory of anthropogenic sources for China and the uncertainty in spatial and temporal distribution of OBB emissions due to satellite

detection limit, we believe the model performance with the constrained OBB emissions was improved and acceptable. The NMB and NME between observed and simulated CO concentrations are shown in Table S15 in the supplement. Similar to $PM_{2.5}$ and $PM_{10}$, the NMBs and NMEs between observed and simulated CO concentrations with constrained OBB emissions were smaller than those with FRP-based OBB emissions or without OBB emissions, implying the advantage of constrained OBB emissions against other inventories.

### 3.3 Comparisons of different methods and studies

We selected CO to compare emissions in this work and other inventories for YRD, given the similar emission factors of CO applied in different studies. CO emissions from the three methods in this study were compared with GFASv1.0 (Kaiser et al., 2012), GFEDv3.0 (van der Werf et al., 2010), GFEDv4.1 (Randerson et al. 2018), Wang and Zhang (2008), Huang et al. (2012), Xia et al. (2016) and Zhou et al. (2017a), as shown in Figure 6. The emissions from Wang and Zhang (2008), Huang et al. (2012), Xia et al. (2016) and Zhou et al. (2017a) were derived by traditional bottom-up method, while GFASv1.0, GFEDv3.0 and GFEDv4.1 were based on FRP and BA methods. In particular, emissions from small fires were included in GFEDv4.1. Similar inter-annual variations were found for emissions derived from FRP measurement including the constrained and FRP-based emissions in this work, GFAS v1.0, and GFED v4.1, while those of GFEDv3.0 and Xia et al. (2016) were different. The percentages of CRBF were assumed unchanged during the studying period in Xia et al. (2016), thus the temporal variation of OBB emissions were associated with the change in annual straw production.

The constrained CO emissions in this work were lower than other studies using traditional bottom-up method (Wang and Zhang, 2008; Huang et al., 2012; Xia et al., 2016) and higher than those based on burned area and FRP derived from satellite (GFEDv3.0; GFASv1.0; GFEDv4.1). In particular, the average annual constrained emissions from 2005 to 2012 were 3.9, 0.5 and 15.0 times larger than those in GFASv1.0, GFEDv4.1s and GFEDv3.0, respectively. The constrained emissions were closest to GFED v4.1s that included small fires. Since the area of farmland belonging to individual farmers was usually small, small fires were expected to be important sources of OBB emissions in YRD. GFEDv4.1s might still underestimate OBB emissions due to the omission errors for the small fires in MODIS active fire detection

products (Schroeder et al., 2008). In addition, the constrained CO emission for 2013 was 31.5% larger than those by Qiu et al. (2016) calculated based on burned area from satellite observations. The average annual CO emissions from 2005 to 2012 by the constraining method were 57.2% smaller than Xia et al. (2016), and the constrained emissions for 2006 were respectively 27.6% and 56.9% lower than those by Huang et al. (2012) and Wang and Zhang (2008). It implied again that the emissions derived from traditional bottom-up method might be overestimated. Moreover, discrepancy in estimations for the same year between Huang et al. (2012) and Wang and Zhang (2008) with traditional bottom-up resulted mainly from application of different percentages of CRBF, implying that calculation of OBB emissions was sensitive to the parameter with the bottom-up approach.

The spatial distribution of constrained emissions in this work and those in GFASv1.0, GFEDv3.0 and GFEDv4.1s were illustrated in Figure 7. Intensive OBB emissions in GFEDv3.0 were mainly found in parts of Anhui, Jiangsu and Shanghai, while the constrained emissions, GFEDv4.1s and GFASv1.0 emissions occurred in most YRD regions in accordance with the distribution of fire points. Therefore, GFEDv3.0 might miss a large number of burned areas, leading to underestimation in emissions and bias in spatial distribution.

In order to understand the discrepancies of emissions for different species in this work and other inventories, the emissions of 2010 derived from the three methods in this study, GFASv1.0, GFEDv3.0, GFEDv4.1s and Xia et al. (2016) were summarized in Table 3. Similar to CO, the constrained emissions for all species in this work were lower than Xia et al. (2016) and OBB emissions of this study based on traditional bottom-up method. The constrained emissions for all species in this work were larger than GFASv1.0 and those for all species except $NH_3$ were larger than GFEDv3.0 and GFEDv4.1s. In addition, the constrained emissions for most species were lower than the emissions from Huang et al. (2012), Wang and Zhang (2008) and Xia et al. (2016) using traditional bottom-up method in 2006. In most cases, the discrepancy in activity levels between studies was larger than that in emission factors. Specifically, the OBB emissions for all species in FRP-based (WSE) were smaller than those derived by bottom-up method. The differences in OBB emissions between bottom-up and FRP-based (WSE) method were larger than 50% of those between the bottom-up and the original FRP-based method with different emission factors for most species. It

indicated that the discrepancy in activity levels contributed the most to the difference in OBB emissions between the two methods.

Resulting from the different sources of emission factors, the discrepancies between studies or methods varied greatly by species. For $PM_{10}$ and $PM_{2.5,}$ as an example, the emissions by Xia et al. (2016) were respectively 35.8% and 50.3% higher than constrained emissions in 2010. The discrepancies for $SO_2$ and $NO_X$ were larger: the emissions by Xia et al. (2016) were 4.7 and 3.1 times larger than our constrained emissions, respectively. Moreover, the constrained NMVOCs emission was 152.5 and 10.7 times larger than that of GFEDv3.0 and GFEDv4.1s in 2010, as the emission factors of GFEDv3.0 and GFEDv4.1s did not contain oxygenated VOCs. In contrast, the constrained $NH_3$ emission was 4.7% and 47.9% smaller than that of GFEDv3.0 and GFEDv4.1s. The comparisons indicated that emission factors were important sources of uncertainties in estimation of OBB emissions with different methods.

### 3.4 Contribution of OBB to particulate pollution and its influencing factors

The brute-force method (BFM, Dunker et al., 1996) was used to analyze the contributions of OBB to $PM_{10}$ pollution for the two OBB events, June 17-24, 2010 and June 8-14, 2012. Simulated $PM_{10}$ concentrations with and without constrained OBB emissions were compared, and the difference indicated the contribution from OBB as shown by city in Figure 8. The average contribution in June 8-14, 2012 was estimated at 37.6% (56.7 $\mu g/m^3$) for 22 cities in YRD, and the contribution for June 17-24, 2010 was smaller at 21.8 % (24.0 $\mu g/m^3$) for 17 cities. Our result for 2012 was nearly the same as that for 5 YRD cities in 2011 (37.0%) by Cheng et al. (2014). Using the BFM method, the contribution of OBB emissions to $PM_{10}$ concentrations were estimated to increase by 136.3% from 2010 to 2012 in this work, and the growth rate was larger than that of OBB emissions (50.8%). Therefore, factors other than emissions (e.g., meteorology) could also play an important role in elevating the contribution of OBB to ambient particle pollution. For example, the average precipitation in June 8-14, 2012 was 36% lower than that in June 17-24, 2010, exaggerating the particle pollution during OBB event. For the OBB event during June 7-13, 2014, the contributions of OBB to both $PM_{2.5}$ and $PM_{10}$ concentrations were shown by city in Figure 9. The average contributions of $PM_{2.5}$ and $PM_{10}$ were estimated at 29% and 23% for 22 cities in YRD, indicating again that the OBB was an

important source of ambient particles. OBB contribution to $PM_{10}$ for 2014 was smaller than that for 2012, attributed mainly to the reduced straw burning in crop land.

The average contributions of OBB for 2012 were estimated at 55.0% (98.4 $\mu g/m^3$), 36.4% (58.0 $\mu g/m^3$), 23.6% (12.9 $\mu g/m^3$), and 14.4% (11.2 $\mu g/m^3$) for 6 cities of Anhui, 10 cities of Jiangsu, 5 cities of Zhejiang and Shanghai, respectively. For individual cities, large contributions of OBB for 2012 were found in Xuzhou, Bozhou, Fuyang, and Lianyungang located in north YRD, reaching 82.3% (284.3 $\mu g/m^3$), 75.2% (207.5 $\mu g/m^3$), 71.9% (134.7 $\mu g/m^3$) and 63.5% (96.2 $\mu g/m^3$), respectively. Similarly, large contributions for 2010 were found in Lianyungang, Fuyang and Bozhou reaching 63.3% (69.8 $\mu g/m^3$), 58.2% (71.9 $\mu g/m^3$) and 78.8% (53.6 $\mu g/m^3$), respectively. In general the spatial distribution of contributions to $PM_{10}$ mass concentrations was similar with that of fire points, confirming the rationality of constraining OBB emissions with observed $PM_{10}$ concentration in cities in north Anhui and Jiangsu. For $PM_{2.5}$, the large contributions of OBB were found in Xuzhou, Huaian and Suqian during the event in 2014, reaching 67.5% (111.7 $\mu g/m^3$), 60.7% (50.6 $\mu g/m^3$) and 53.2% (49.6 $\mu g/m^3$), respectively.

To explore the influence of meteorology on air pollution caused by OBB, we simulated $PM_{10}$ concentrations for June 8-14 (PE1) and June 22-28 2012 (PE2) with varied meteorology conditions but fixed OBB emissions (i.e., constrained emissions for June 8-14, 2012). Poorer meteorology conditions during PE1 were found than PE2. The average wind speed in PE1 was 2.4 m/s, 17% lower than that in PE2. The average wind direction in PE1 was 168.3 °, close to south with polluted air in land. In contrast, the average wind direction in PE2 was 118.3 °, close to east with clean air from the ocean. The average precipitation in PE2 was 6.8mm, 28% higher than that in PE1. As shown in Figure 10, the average contribution of OBB to $PM_{10}$ concentrations for 22 cities in YRD region was estimated at 56.7 $\mu g/m^3$ for PE1, 23% larger than that for PE2, and the contributions in most cities were much larger for PE1 than those for PE2, except for Bozhou and Fuyang. The comparisons thus suggest that air pollution caused by OBB would exaggerate under poorer meteorology conditions. To reduce air pollution caused by OBB in harvest season in YRD, therefore, more attention should be paid to the OBB restriction on those days with unfavorable meteorology conditions such as calm wind and rainless period.

To further analyze the influence of diurnal variation of emissions on air pollution caused by OBB, we simulated $PM_{10}$ concentrations of June 17-24 2010 with various diurnal curves of OBB emissions (i.e., those for 2010 and 2012). Constrained emissions were applied in the simulation. As shown in Figure 11, the contributions of OBB to $PM_{10}$ concentrations based on diurnal curve of 2012 were larger than those based on 2010 for almost all YRD cities, and the average contribution for the 17 cities was calculated at 28.6 $\mu g/m^3$ based on diurnal curve of 2012, 10% larger than that based on 2010. The contribution in Bozhou changed most (1.37 times larger with 2012 curve), while those in Shanghai, Huzhou and Shaoxing changed least. The time of peak value for OBB emissions in 2012 was 2.5 hours later than 2010, indicating that the fraction of OBB emissions at night for 2012 would be larger than that for 2010. As the diffusion condition for air pollutants at night was usually worse than that during daytime, more OBB emissions at night would elevate its contribution to particle pollution. In the actual fact, the supervision of OBB prohibition was usually conducted by government during daytime, thus some farmers burned more crop residues at night to avoid the punishment. To improve the air quality in harvest season in YRD, more attention should be paid to the OBB restriction at night.

### 3.5 Uncertainty analysis

The uncertainties of OBB emissions estimated with bottom-up and FRP-based methods were quantified by species using a Monte-Carlo simulation for 2012. A total of 20,000 simulations were performed and the uncertainties were expressed as 95% confidence intervals (CIs) around the central estimates. The parameters contributing most to OBB emission uncertainty were also identified according to their contribution to the variance in Monte-Carlo simulation.

For traditional bottom-up method, parameters included crop productions, percentages of CRBF, straw to grain ratios, combustion efficiencies, and emission factors. Crop production was directly taken from official statistical yearbooks (NBS, 2013) and its uncertainty was expected to be limited and not included in the analysis. As the percentage of CRBF was determined at half of the percentage of unused crop residues, its uncertainty was set at -100% to +100%. The combustion efficiencies were assumed within an uncertainty range of 10% around the mean value according to de Zarate (2005) and Zhang et al. (2008). Uncertainties of emission factors were obtained from original literatures where they were derived. If emission factor was

673 derived from a single measurement, normal distribution was applied with standard
674 deviation directly taken from that work. If emission factor was derived from multiple
675 measurements and the samples were insufficient for data fitting, uniform distribution
676 was tentatively applied with a conservative strategy to avoid possible underestimation
677 of uncertainty: The uncertain range of given emission factor would be expanded
678 according to Li et al. (2007) if the range originally from multiple studies was smaller
679 than that in Li et al. (2007). Summarized in Table S16 in the supplement was a
680 database for emission factors and percentages of CRBF, with their uncertainties
681 indicated by probability distribution function (PDF). As shown in Table 4, the
682 uncertainties of OBB emissions with traditional bottom-up method for $PM_{10}$, $PM_{2.5}$,
683 EC, OC, $CH_4$, NMVOCs, CO, $CO_2$, $NO_X$, $SO_2$ and $NH_3$ in 2012 were estimated at
684 -56% to +70%, -56% to +70%, -50% to +54%, -54% to +73%, -49% to +58%, -48%
685 to +59%, -46% to +73%, -48% to +60%, -47% to +87%, -59% to +138% and -51% to
686 +67%, respectively. For most species, the percentages of CRBF contributed largest to
687 the uncertainties of OBB emissions, while emission factors were more significant to
688 $SO_2$ uncertainty.

689 For FRP-based method, parameters included total FRE, combustion conversion
690 ratio and emission factors. Uncertainty of total FRE was associated with FRP value,
691 MODIS detection resolution, and the methodology used to calculate FRE per fire
692 pixel. Indicated by Freeborn et al. (2014), the coefficient of variation of MODIS FRP
693 for a fire pixel was 50%, but it declined to smaller than 5% for the aggregation of over
694 50 MODIS active fire pixels. Give the large number of fire pixels for in YRD (more
695 than 17000 in 2012), FRP was expected to contribute little to uncertainty of total FRE
696 and could thus be ignored. Due to limitation of MODIS resolution and limited
697 overpass times, many fires could not be detected and the number of fire pixel could be
698 underestimated by 300% on crop-dominant areas (Schroeder et al., 2008), therefore
699 the uncertainty of number of fire pixel was assumed to be 0 to +300%. The method
700 used to calculate FRE based on single fire pixel assumed that fire lasted one day.
701 Given the small cropland owned by one farmer in YRD, individual fire normally
702 lasted several hours, and FRE could be overestimated. As the total FRE in FRP-based
703 method was estimated 2.6 times larger than that from constraining method based on
704 the same number of the fire pixel, we tentatively assumed the uncertainty range of
705 FRE for one fire pixel at 0% to -72%. The uncertainty of total FRE was then
706 estimated at -17% to +154% (95% CIs) based on the principle that total FRE was

calculated as the number of fire pixel multiplied by average FRE. The uncertainty of combustion conversion ratio was derived from Wooster et al. (2005) and Freeborn et al. (2008), while those of emission factors taken from Akagi et al. (2011). As a result, uncertainties of FRP-based inventory were estimated at -77% to +274%, -63% to +244%, -78% to +281%, -78% to 276%, -83% to +315%, -63% to +243%, -52% to +223%, -21% to +164%, -82% to +303%, -78% to +279%, and -82% to +302% for $PM_{10}$, $PM_{2.5}$, EC, OC, $CH_4$, NMVOCs, CO, $CO_2$, $NO_X$, $SO_2$ and $NH_3$ in 2012, respectively. Emission factors contributed most to the uncertainties of emissions for all species except $CO_2$.

The uncertainty of constrained emissions could hardly be provided by Monte-Carlo simulation, as the results were associated with CTM performance. In general, CTM performance could be influenced by emission estimates for sources other than OBB, chemistry mechanism of CTM and temporal and spatial distribution of OBB emissions. Emission inventory of anthropogenic sources that incorporates the best available information of individual plants was expected to improve the CTM performance at the regional or local scale (Zhou et al., 2017b). The influence of chemistry mechanism came mainly from secondary organic carbon (SOC) modeling. According to the Cheng et al. (2014) and Chen et al. (2017), the mass fraction of SOC to $PM_{10}$ could reach 10% during the OBB event in YRD, and that part might not be well constrained with the approach we applied in this work. Similar to FRP-based method, moreover, temporal and spatial distribution of OBB emissions based on FRP might not be entirely consistent with the reality, due to omission errors in the MODIS active fire detection products and limited times of satellite overpass as discussed earlier. Due to data limitation, finally, we relied on available $PM_{10}$ concentrations in current method. More data of multi pollutant concentrations (e.g., $PM_{2.5}$, OC and EC) with sufficient temporal and spatial resolution are in great need to better constrain the OBB emissions.

In general, uncertainties of OBB emissions with traditional bottom-up method were estimated smaller than those with FRP-based method, and uncertainties for $CO_2$ and CO were usually smaller than other species in both methods attributed mainly to fewer variations in their emission factors. OBB emission estimation with traditional bottom-up method could be improved if more accurate percentages of CRBF are obtained, and that with FRP-based method could be improved when the omission error of satellite and the uncertainties of emission factors are reduced. Efforts should

741 also be recommended on improvement of CTM for better constraining the OBB
742 emissions.
743

744 ## 4. Conclusions

745 Taking YRD in China as an example, we have thoroughly analyzed the
746 discrepancies and their sources of OBB emissions estimated with traditional
747 bottom-up, FRP-based and constraining methods. The simulated $PM_{10}$ concentrations
748 through CMAQ with constrained emissions were closest to available observation,
749 implying the improvement of emission estimation with this method. The inter-annual
750 variations in emissions with FRP-based and constraining methods were similar with
751 the fire counts, while that with traditional bottom-up method was not. It indicated that
752 emissions with traditional bottom-up method could not capture the real inter-annual
753 trend of OBB emissions. The emissions of all species except NMVOCs based on
754 traditional bottom-up method might be overestimated in most years, attributed mainly
755 to the elevated percentages of CRBF used in the method. The emissions with
756 FRP-based method might be underestimated in 2005-2015, attributed to the omission
757 errors in the MODIS active fire detection products and thereby to the underestimation
758 in mass of CRBF. The CO emissions with traditional bottom-up, FRP-based and
759 constraining methods were compared with other studies. Similar temporal variations
760 were found for the constrained emissions, emissions based on FRP-based, and
761 emissions in GFASv1.0 and GFEDv4.1s. CO emissions based on traditional
762 bottom-up method both in this work and other studies were usually higher than those
763 derived by constraining method, and the CO emissions based on FRP-based method
764 both in this work and other studies usually were lower than those derived by
765 constraining method. It again demonstrated that traditional bottom-up method might
766 overestimate OBB emissions in YRD and FRP-based method might underestimate
767 them. The contributions of OBB to particulate pollution in typical episodes were
768 analyzed using the Brute-force method in CMAQ modeling. The OBB emissions in
769 2012 were 51% larger than those in 2010, while its contribution to average $PM_{10}$ mass
770 concentrations was estimated to increase by 136% from 2010 to 2012. It indicated that
771 the elevated contribution of OBB was not attributed only to growth in OBB emissions
772 but was also influenced by the meteorology. Quantified with a Monte-Carlo
773 framework, the uncertainties of OBB emissions with traditional bottom-up method

were smaller than those with FRP-based method. The uncertainties of emissions based on traditional bottom-up and FRP-based were mainly from the percentages of CRBF and emission factors, respectively. Further improvement on CTM for OBB events would help better constraining OBB emissions.

Limitations remained in this study. Given the difficulty in field investigation, annual CRBF used in traditional bottom-up method was obtained from limited studies and it could not correctly reflect the real OBB activity. The reliability of OBB emissions with FRP-based method depended largely on the detection resolution of the satellite. In YRD where the burned areas of individual fires were small, many fires could not be detected by MODIS. The accuracy of constrained emissions depended largely on model performance and spatial and temporal distributions of OBB emissions derived from satellite-observed FRP. Therefore FRP-based and constraining method may be improved if more reliable fire information is obtained. In addition, more measurements on local emission factors for OBB are suggested in the future to reduce the uncertainty of emissions.

## Acknowledgements

This work was sponsored the National Key Research and Development Program of China (2016YFC0201507 and 2017YFC0210106), Natural Science Foundation of China (91644220 and 41575142), Natural Science Foundation of Jiangsu (BK20140020), and Special Research Program of Environmental Protection for Common wealth (201509004). The MCD14ML data were provided by LANCE FIRMS operated by the NASA/GSFC/Earth Science Data and Information System (ESDIS) with funding provided by NASA/HQ.

## References

Akagi, S., Yokelson, R. J., Wiedinmyer, C., Alvarado, M., Reid, J., Karl, T., Crounse, J., and Wennberg, P.: Emission factors for open and domestic biomass burning for use in atmospheric models, Atmos. Chem. Phys. 11 (9), 4039-4072, 2011.

Andreae, M. O., and Merlet, P.: Emission of trace gases and aerosols from bio mass burning, Glob. Biogeochem. Cy. 15(4), 955-966. http://dx.doi.org/10.1029/2000gb001382, 2001.

Bi, Y. Y.: Study on straw resources evaluation and utilization, Chinese Academy Agriculture Sciences, Beijing, China, 2010 (in Chinese).

Cao, G. L., Zhang, X. Y., Wang, D., and Zheng, F. C.: Inventory of atmospheric pollutants discharged from open biomass burning in China continent, Chinese Science Bulletin, 52(15):1826-1831, 2007 (in Chinese).

Chen, D., Cui H. F., Zhao Y., Yin L., Lu, Y., Wang, Q. G.: A two-year study of carbonaceous aerosols in ambient PM 2.5 at a regional background site for western Yangtze River Delta, China, Atmos. Res., 183, 351-361, 2017.

Cheng, Z., Wang, S.X., Fu, X., Watson, J.G., Jiang, J., Fu, Q., Chen, C., Xu, B., Yu, J., Chow, J.C., and Hao, J.: Impact of biomass burning on haze pollution in the Yangtze River delta, China: a case study in summer 2011, Atmos. Chem. Phys., 14, 4573-4585, 2014.

Cheng, Z., Wang, S.X., Jiang, J. K., Fu, Q.Y., Chen, C.H., Xu, B.Y., Yu J.Q., Fu, X., and Hao J.M.: Long-term trend of haze pollution and impact of particulate matter in the Yangtze River Delta, China, Environ. Pollut., 182, 101-110, 2013.

Crutzen, P. J., and Andreae, M. O.: Biomass burning in the tropics: Impact on atmospheric chemistry and biogeochemical cycles, Science, 250 (4988), 1669-1678, 1990.

Davies, D. K., Ilavajhala, S., Wong, M. M., and Justice, C. O.: Fire Information for Resource Management System: Archiving and Distributing MODIS Active Fire Data, IEEE Geosci. Remote Sens., 47, 72-79, 2009.

de Zarate, I. O., Ezcurra, A., Lacaux, J. P., Van Dinh, P., de Argandona, J. D.: Pollution by cereal waste burning in Spain, Atmos. Environ., 73, 161~170, 2005.

Dunker, A. M., Morris, R. E., Pollack, A. K., Schleyer, C. H., and Yarwood, G.: Photochemical modeling of the impact of fuels and vehicles on urban ozone using auto oil program data, Environ. Sci. & Technol., 30, 787–801, 1996.

Emery, C., Tai, E., and Yarwood, G.: Enhanced meteorological modeling and performance evaluation for two Texas episodes, Report to the Texas Natural Resources Conservation Commission, prepared by ENVIRON, International Corp, Novato, CA, 2001.

European Space Agency and Université Catholique de Louvain, GLOBCOVER 2009 Products Description and Validation Report, 2011, Available online: http://due.esrin.esa.int/files/GLOBCOVER2009_Validation_Report_2.2.pdf.

Fu, X., Wang, S.X., Zhao, B., Xing, J., Cheng, Z., Liu, H., and Hao, J. M.: Emission inventory of primary pollutants and chemical speciation in 2010 for the Yangtze River Delta region, China, Atmos. Environ., 70, 39-50, 2013.

Freeborn, P. H., Wooster, M. J., Roy, D. P., Cochrane, M. A.: Quantification of MODIS fire radiative power (FRP) measurement uncertainty for use in satellite based active fire characterization and biomass burning estimation, Geophys. Res. Lett., 41(6), 1988-1994, 2014.

Freeborn, P. H., Wooster, M. J., Hao, W. M., Ryan, C. A., Nordgren, B. L., Baker, S. P., and Ichoku, C.: Relationships between energy release, fuel mass loss, and trace gas and aerosol emissions during laboratory biomass fires, J. Geophys. Res., 113, D01301. http://dx.doi.org/10.1029/2007jd008679, 2008.

Giglio, L., Randerson, J. T., and van der Werf, G. R.: Analysis of daily, monthly, and annual burned area using the fourth generation global fire emissions database (GFED4), J. Geophys. Res.: Biogeo., 118, 317–328, doi:10.1002/jgrg.20042, 2013.

Giglio, L., Descloitres, J., Justice, C. O., Kaufman Y. J.: An enhanced contextual fire detection algorithm for MODIS, Remote Sens. Environ., 87(2-3): 273-282, 2003.

Guo, H., Cheng, T., Gu, X., Wang, Y., Chen, H., Bao, F., Shi, S. Y., Xu, B. R., Wang, W. N., Zuo, X., Zhang, X. C., Meng, C.: Assessment of $pm_{2.5}$ concentrations and exposure throughout china using ground observations, Sci. Total Environ., 1024, 601-602, 2017.

Hodzic A., Duvel J. P.: Impact of biomass burning aerosols on the diurnal cycle of convective clouds and precipitation over a tropical island, J. Geophys. Res., 123, 1017–1036. https://doi.org/10.1002/2017JD027521, 2018.

Hooghiemstra, P. B., Krol, M. C., vanLeeuwen, T. T., van der Werf, G. R., Novelli, P. C., Deeter, M. N., Aben, I., and Röckmann, T.: Interannual variability of carbon monoxide emission estimates over South America from 2006 to 2010, J. Geophys. Res., 117, D15308, doi:10.1029/2012JD017758, 2012.

Huang, X., Ding, A. J., Liu, L. X., Liu, Q., Ding, K., Nie, W., Xu, Z., Chi, X. G., Wang, M. H., Sun, J. N., Guo, W. D., and Fu, C. B.: Effects of aerosol-radiation interaction on precipitation during biomass-burning season in East China, Atmos. Chem. Phys. Discuss., doi: 10.5194/acp-2016-272, 2016.

Huang, X., Li M., Li, J., Song, Y.: A high-resolution emission inventory of crop burning in fields in China based on MODIS Thermal Anomalies/Fire products, Atmos. Environ., 50(3), 9-15, 2012.

Jiangsu Provincial Development and Reform Commission (JPDRC), and Jiangsu Provincial Agricultural Commission (JPAC): Comprehensive utilization planning of crop straw in Jiangsu, Nanjing, China, 2009 (in Chinese).

Jiménez, P., Jorba, O., Parra R. and Baldasano J. M.: Evaluation of MM5-EMICAT2000-CMAQ performance and sensitivity in complex terrain: High-resolution application to the northeastern Iberian Peninsula, Atmos. Environ., 40, 5056-5072, doi:10.1016/j.atmosenv.2005.12.060, 2006.

Kaiser, J. W., Heil, A., Andreae, M. O., Benedetti, A., Chubarova, N., Jones, L., Morcrette, J. J., Razinger, M., Schultz, M. G., Suttie, M., and van der Werf,G. R.: Biomass burning emissions estimated with a global fire assimilation system based on observed fire radiative power, Biogeosciences, 9, 527–554, doi: 10.5194/bg-9-527-2012, 2012.

Konovalov, B., Berezin, E. V., Ciais, P., Broquet, G., Beekmann, M., Hadji-Lazaro, J., Clerbaux, C., Andreae, M. O., Kaiser, J. W., and Schulze, E.-D.: Constraining $CO_2$ emissions from open biomass burning by satellite observations of co-emitted species: a method and its application to wildfires in Siberia, Atmos. Chem. Phys., 14, 10383–10410, 2014.

Kota S. H., Guo H., Myllyvirta L., Hu J. L., Sahu S. K., Garaga R., Ying Q., Gao A. F., Dahiya S., Wang Y., Zhang H. L.: Year-long simulation of gaseous and particulate air pollutants in India, Atmos. Environ., 180, 244-255, doi:10.10 16/j.atmosenv.2018.03.003, 2018.

Krol, M., Peters, W., Hooghiemstra, P., George, M., Clerbaux, C., Hurtmans, D., McInerney, D., Sedano, F., Bergamaschi, P., El Hajj, M., Kaiser, J. W., Fisher, D., Yershov, V., and Muller, J.-P.: How much CO was emitted by the 2010 fires around Moscow?, Atmos. Chem. Phys., 13, 4737–4747, doi: 10.5194/acp-13-4737-2013, 2013.

Li, J. F., Song, Y., Mao, Y., Mao, Z. C., Wu, Y. S., Li, M. M., Huang, X., He, Q. C., and Hu, M.: Chemical characteristics and source apportionment of $PM_{2.5}$ during the harvest season in eastern China's agricultural regions, Atmos. Environ., 92, 442–448, doi: 10.1016/j.atmosenv.2014.04.058, 2014.

Li, X. H.,Wang, S. X., Duan, L., Hao, J. M., LiC., Chen, Y. S., and Yang, L.: Particulate and trace gas emissions from open burning of wheat straw and corn stover in China, Environ. Sci.& Technol., 41, 6052-6058, 2007.

Liu, M. X., Song, Y., Yao H., Kang, Y. N., Li, M. M., Huang, X., and Hu, M.: Estimating emissions from agricultural fires in the North China Plain based on MODIS fire radiative power, Atmos. Environ., 112, 326–334, 2015.

National Bureau of Statistics (NBS): China Statistical Yearbook 2006-2013, China Statistics Press, Beijing, 2013 (in Chinese).

National Development and Reform Commission Office (NDRC), and National Environmental Protection Department (NEPD): Comprehensive utilization and burning of crop straw in China, Beijing, China, 2014 (in Chinese).

Price, C., Penner, J., and Prather, M.: $NO_x$ from lightning, Part I: Global distri bution based on lightning physics, J. Geophys. Res.-Atmos., 102, D5, doi: 10.1 029/96JD03504, 1997.

Qiu, X. H., Duan, L, Chai F. H. Wang S. X., Yu Q., and Wang S. L.: Deriving high-resolution emission inventory of open biomass burning in China based on satellite observations, Environ. Sci. Technol., 50 (21), 11779–11786. DOI: 10.1021/acs.est.6b02705, 2016.

Ran, L., Zhao, C., Geng, F., Tie, X., Peng, L., Zhou, G., Yu, Q., Xu, J., and Guenther, A.: Ozone photochemical production in urban Shanghai, China: Anal ysis based on groud level observations, J. Geophys. Res., 114, D15301, doi: 10. 1029/2008JD010752, 2009.

Randerson, J. T., van der Werf, G. R., Giglio, L., Collatz, G. J., and Kasibhatla, P. S.: Global Fire Emissions Database, Version 4.1, (GFEDv4), ORNL DAAC, Oak Ridge, Tennessee, USA. http://dx.doi.org/10.3334/ORNLDAAC/1293, 2018.

Richter, A., Burrows, J. P., Nuss, H., Granier, C., and Niemeier, U.: Increase in tropospheric nitrogen dioxide over China observed from space, Nature, 437, 129-132, 2005.

Schroeder, W., Prins, E., Giglio, L., Csiszar, I., Schmidt, C., Morisette, J., and Morton, D.: Validation of GOES and MODIS active fire detection products usi ng ASTER and ETM+ data, Remote Sens. Environ, 112 (5), 2711-2726, http:// dx.doi.org/10.1016/j.rse.2008.01.005, 2008.

Shi, Y. S., and Yamaguchi, Y.: A high-resolution and multi-year emissions inventory for biomass burning in Southeast Asia during 2001-2010, Atmos. Environ., 98 (98): 8-16, 2014.

938 Sindelarova, K., Granier, C., Bouarar, I., Guenther, A., Tilmes, S., Stavrakou, T.,
939 Müller, J.-F., Kuhn, U., Stefani, P., and Knorr, W.: Global data set of biogenic VOC
940 emissions calculated by the MEGAN model over the last 30 years, Atmos. Chem.
941 Phys., 14, 9317–9341, doi: 10.5194/acp-14-9317-2014, 2014.

942 Streets, D. G., and Yarber, K. F.: Biomass burning in Asia: Annual and seasonal
943 estimates and atmospheric emissions, Global Biogeochemical Cycles, 17, 4, 1099, doi:
944 10.1029/2003GB002040, 2003.

945 Su, J. F., Zhu B., Kang, H. Q., Wang, H. N., and Wang T. J.: Applications of pollutants
946 released form crop residues at open burning in Yangtze River Delta, Environmental
947 Science, 5, 1418-1424, 2012 (in Chinese).

948 van der Werf, G. R., Randerson, J. T., Giglio, L., Collatz, G. J., Mu, M., Kasi
949 bhatla, P. S., Morton, D. C., DeFries, R. S., Jin, Y., and van Leeuwen, T. T.:
950 Global fire emissions and the contribution of deforestation, savanna, forest, agri
951 cultural, and peat fires (1997-2009), Atmos. Chem. Phys., 10, 11707-11735, doi:
952 10.5194/acp-10-11707-2010, 2010.

953 Van Donkelaar, A., Martin, R. V., Brauer, M., Kahn, R., Levy, R., Verduzco, C., and
954 Villeneuve, P. J.: Global estimates of ambient fine particulate matter concentrations
955 from satellite-based aerosol optical depth: development and application, Environ.
956 Health. Persp., 118, 847-855, 2010.

957 Vermote, E., Ellicott, E., Dubovik, O., Lapyonok, T., Chin, M., Giglio, L., and
958 Roberts, G.J.: An method to estimate global biomass burning emissions of organic and
959 black carbon from MODIS fire radiative power, J. Geophys. Res. 114 (D18)
960 http://dx.doi.org/10.1029/2008jd011188, 2009.

961 Wang, S. X., and Zhang, C. Y.: Spatial and temporal distributions of air pollutant
962 emissions from open burning of crop residues in China, Sciencepaper Online,
963 5(5):329-333, 2008 (in Chinese).

964 Wiedinmyer, C., Akagi, S. K., Yokelson, R. J., Emmons, L. K., Al- Saadi, J. A.,
965 Orlando, J. J., and Soja, A. J.: The Fire Inventory from NCAR (FINN): a high
966 resolution global model to estimate the emissions from open burning, Geosci. Model
967 Dev., 4, 625–641, doi: 10.5194/gmd-4-625-2011, 2011.

968 Wooster, M. J., Roberts, G., Perry, G. L. W., and Kaufman, Y. J.: Retrieval of biomass
969 combustion rates and totals from fire radiative power observations: FRP derivation
970 and calibration relationships between biomass consumption and fire radiative energy
971 release, J. Geophys. Res., 110, D24. http://dx.doi.org/10.1029/2005jd006318, 2005.

972 Xia, Y. M., Zhao Y., Nielsen, C. P.: Benefits of China's efforts in gaseous pollutant
973 control indicated by the traditional bottom-up emissions and satellite observations
974 2000-2014, Atmos. Environ., 136: 43-53, 2016.

975 Xiao, Z. M., Zhang, Y. F., Hong, S. M., Bi, X. H., Jiao, L., Feng, Y. C., and Wang, Y.
976 Q.: Estimation of the main factors influencing haze, based on a long-term monitoring
977 Campaign in Hangzhou, China. Aerosol Air Qual. Res., 11, 873-882, 2011.

978 Xing, J., Mathur, R., Pleim, J., Hogrefe, C., Gan, C. -M., Wong, D. C., Wei, C.,
979 Gilliam, R. and Pouliot, G.: Observations and modeling of air quality trends over
980 1990–2010 across the Northern Hemisphere: China, the United States and Europe,
981 Atmos. Chem. Phys., 15, 2723-2747, 2015.

982 Zhang, H. F., Ye, X. G., Cheng, T. T., Chen, J. M., Yang, X., Wang, L., and Zhang, R.

983 Y.: A laboratory study of agricultural crop residue combustion in China: Emission
984 factors and emission inventory, Atmos. Environ., 42, 8432-8441, 2008.

985 Zhang, Y., Liu, P., Pun, B., and Seigneur, C.: A comprehensive performance
986 evaluation of MM5-CMAQ for the Summer 1999 Southern Oxidants Study
987 episode-Part I: Evaluation protocols, databases, and meteorological predictions,
988 Atmos. Environ., 40, 4825–4838, 2006.

989 Zhao Y., Zhang J., and Nielsen C.P.: The effects of recent control policies on trends in
990 emissions of anthropogenic atmospheric pollutants and $CO_2$ in China, Atmos. Chem.
991 Phys., 13, 487-508, 2013.

992 Zheng, Y., Xue, T., Zhang, Q., Geng, G., Tong, D., Li, X. and He, K. B.: Air quality
993 improvements and health benefits from China's clean air action since 2013, Environ.
994 Res. Lett., 12, 114020, 2017.

995 Zhou Y., Xing X. F., Lang J. L., Chen D. S., Cheng S. Y., Wei L., Wei X., and Liu C.:
996 A comprehensive biomass burning emission inventory with high spatial and temporal
997 resolution in China, Atmos. Chem. Phys., 17, 2839–2864, 2017a.

998 Zhou, Y. D., Zhao Y., Mao P., Zhang Q, Zhang J., Qiu, L. P., and Yang, Y.:
999 Development of a high-resolution emission inventory and its evaluation and
1000 application through air quality modeling for Jiangsu Province, China, Atmos. Chem.
1001 Phys., 17, 211–233, 2017b.

## FIGURE CAPTIONS

**Figure 1. (a) spatial patterns of fire points in June 2010 and June 2012, (b) $PM_{10}$ concentrations for city-level in YRD in June 2010 and June 2012, and (c) temporal variations of daily fire occurrences in June 2010 and 2012. City abbreviations FY, BZ, BB, HN, HF, CZ(a), XZ, LYG, NJ, YZ, ZJ, TZ, NT, CZ, WX, SZ, HZ(a), JX, HZ, SX, NB, SH indicate is Fuyang, Bozhou, Bengbu, Huainan, Hefei, Chuzhou, Xuzhou, Lianyungang, Nanjing, Yangzhou, Zhenjiang, Taizhou, Nantong, Changzhou, Wuxi, Suzhou, Huzhou, Jiaxing, Hangzhou, Shaoxing, Ningbo, and Shanghai.**

**Figure 2. Model domain and locations of 43 meteorological monitoring sites. The numbers of 1-41 represent the cities of Fuyang, Bozhou, Huaibei, Suzhou, Huainan, Bengbu, Luan, Hefei, Chuzhou, Anqing, Chaohu, Maanshan, Chizhou, Tongling, Wuhu, Huangshan, Xuancheng, Xuzhou, Lianyungang, Suqian, Huaian, Yancheng, Yangzhou, Taizhou, Nanjing, Zhenjiang, Nantong, Changzhou, Wuxi, Suzhou; Huzhou, Jiaxing, Hangzhou, Shaoxing, Ningbo, Zhoushan, Quzhou, Jinhua, Taizhou, Lishui and Wenzhou, respectively.**

**Figure 3. Fire counts and $CO_2$ emissions estimated with traditional bottom-up, FRP-based and constraining methods for YRD 2005-2012.**

**Figure 4. Observed 24-hour averaged $PM_{10}$ concentrations and simulated hourly $PM_{10}$ concentrations without OBB emissions (No_OBB) and with OBB emissions based on traditional bottom-up (Traditional_OBB), FRP-based (FRP_OBB) and constraining (Constrained_OBB) methods in Lianyungang, Fuyang, Bozhou, Bengbu, Huainan, Hefei, and Chuzhou during June 17-25, 2010.**

**Figure 5. Observed 24-hour averaged $PM_{10}$ concentrations and simulated hourly $PM_{10}$ concentrations without OBB emissions (No_OBB) and with OBB emissions based on traditional bottom-up (Traditional_OBB), FRP-based (FRP_OBB) and constraining (Constrained_OBB) methods in Xuzhou, Lianyungang, Fuyang, Bozhou, Bengbu, Huainan, Hefei, and Chuzhou during June 8-14, 2012.**

**Figure 6. Annual CO emissions from OBB in YRD obtained in this work and other studies from 2005 to 2012.**

**Figure 7. Spatial distributions of CO emissions from OBB obtained in this work (constraining method), GFAS v1.0, GFED v3.0 and GFED v4.1s in 2010**

**(Horizontal resolution: 0.5° ×0.5° ).**

**Figure 8. The contribution of OBB to $PM_{10}$ concentrations for different YRD cities during OBB events in June 2010 and 2012.**

**Figure 9. The contribution of OBB to $PM_{2.5}$ and $PM_{10}$ concentrations for different YRD cities during OBB event in June 2014.**

**Figure 10. $PM_{10}$ concentrations contributed by OBB for different YRD cities in Jun 8-14 (PE1) and June 22-28 (PE2), 2012.**

**Figure 11. $PM_{10}$ concentrations contributed by OBB for different YRD cities based on the diurnal variations of 2010 and 2012 in Jun 8-14, 2010.**

# TABLES

**Table 1. Constrained OBB emissions from 2005 to 2015 in YRD (Unit: Gg).**

| | $PM_{10}$ | $PM_{2.5}$ | EC | OC | $CH_4$ | NMVOCs | CO | $CO_2$ | NOx | $SO_2$ | $NH_3$ |
|---|---|---|---|---|---|---|---|---|---|---|---|
| 2005 | 175.7 | 153.7 | 4.4 | 38.7 | 32.1 | 420.3 | 670.2 | 12011.2 | 22.2 | 2.7 | 4.1 |
| 2006 | 171.3 | 149.9 | 4.3 | 37.8 | 31.3 | 409.9 | 653.7 | 11716.7 | 21.7 | 2.6 | 4.0 |
| 2007 | 219.1 | 191.7 | 5.5 | 48.3 | 40.0 | 524.2 | 835.9 | 14981.9 | 27.7 | 3.4 | 5.1 |
| 2008 | 176.7 | 154.6 | 4.4 | 39.0 | 32.3 | 422.8 | 674.3 | 12085.2 | 22.3 | 2.7 | 4.1 |
| 2009 | 178.8 | 156.4 | 4.5 | 39.4 | 32.6 | 427.7 | 682.0 | 12223.3 | 22.6 | 2.8 | 4.2 |
| 2010 | 257.9 | 225.7 | 6.5 | 58.3 | 47.6 | 624.5 | 987.7 | 17720.3 | 33.0 | 4.0 | 6.1 |
| 2011 | 188.9 | 165.3 | 4.7 | 41.7 | 34.5 | 452.0 | 720.7 | 12917.7 | 23.9 | 2.9 | 4.4 |
| 2012 | 389.0 | 340.4 | 9.6 | 83.6 | 70.2 | 919.4 | 1478.6 | 26473.6 | 48.6 | 6.0 | 9.0 |
| 2013 | 260.7 | 228.1 | 6.5 | 57.5 | 47.6 | 623.8 | 994.7 | 17828.1 | 33.0 | 4.0 | 6.1 |
| 2014 | 332.4 | 290.8 | 8.3 | 73.3 | 60.7 | 795.2 | 1268.1 | 22729.0 | 42.0 | 5.1 | 7.8 |
| 2015 | 109.9 | 96.1 | 2.8 | 24.2 | 20.1 | 262.9 | 419.3 | 7514.6 | 13.9 | 1.7 | 2.6 |

**Table 2. Model performance statistics for concentrations of $PM_{2.5}$ and $PM_{10}$ from observation and CMAQ simulation without OBB emissions (No_OBB) and with OBB emissions based on traditional bottom-up (Traditional_OBB), FRP-based (FRP_OBB) and constraining methods (Constrained_OBB) for the three OBB events of June 2010, 2012 and 2014.**

| | | | No_OBB | | Traditional_OBB | | FRP_OBB | | Constrained_OBB | |
|---|---|---|---|---|---|---|---|---|---|---|
| | | | NMB | NME | NMB | NME | NMB | NME | NMB | NME |
| 2010 | $PM_{10}$ | Daily | -47% | 50% | 11% | 44% | -33% | 41% | -16% | 37% |
| 2012 | $PM_{10}$ | Daily | -60% | 68% | -16% | 45% | -45% | 52% | -10% | 45% |
| 2014 | $PM_{10}$ | Daily | -59% | 59% | | | -54% | 54% | -37% | 42% |
| | | Hourly | -59% | 60% | | | -54% | 57% | -37% | 52% |
| | $PM_{2.5}$ | Daily | -52% | 52% | | | -41% | 42% | -12% | 39% |
| | | Hourly | -52% | 56% | | | -41% | 51% | -13% | 54% |
| Bench-mark | $PM_{10}$ | | | | | | | | -45% | 49% |
| | $PM_{2.5}$ | | | | | | | | -33% | 43% |

Note: [a] from Zhang et al. (2006). NMB and NME were calculated using following equations (*P* and *O* indicate the results from modeling prediction and observation, respectively):

$$NMB = \frac{\sum_{i=1}^{n}(P_i - O_i)}{\sum_{i=1}^{n}(O_i)} \times 100\%; \quad NME = \frac{\sum_{i=1}^{n}|P_i - O_i|}{\sum_{i=1}^{n}(O_i)} \times 100\% \quad .$$

**Table 3. OBB emissions in YRD derived from this work and other studies in 2010 (Unit: Gg).**

| | $PM_{10}$ | $PM_{2.5}$ | EC | OC | $CH_4$ | NMVOCs | CO | $CO_2$ | NOx | $SO_2$ | $NH_3$ |
|---|---|---|---|---|---|---|---|---|---|---|---|
| Traditional (this work) | 362.4 | 317.1 | 9.3 | 85.7 | 67.9 | 154.9 | 1391.8 | 24978.0 | 47.0 | 5.4 | 8.7 |
| FRP-based (this work) | 57.8 | 50.6 | 6.4 | 18.5 | 46.5 | 412.5 | 820.1 | 12718.0 | 24.9 | 3.2 | 17.7 |
| FRP-based (WSE) [1] | 158.6 | 139.1 | 4.1 | 38.5 | 30.1 | 68.7 | 612.8 | 11004.3 | 20.9 | 2.4 | 3.9 |
| Constrained (this work) | 257.9 | 225.7 | 6.5 | 58.3 | 47.6 | 624.5 | 987.7 | 17720.3 | 33.0 | 4.0 | 6.1 |
| GFASv1.0 | - | 17.8 | 1.0 | 9.5 | 15.6 | 88.7 | 196.3 | 3097.8 | 5.1 | 1.0 | 3.1 |
| GFEDv3.0 | - | 3.5 | 0.2 | 1.7 | 3.2 | 4.1 | 39.4 | 701.6 | 1.1 | 0.2 | 6.4 |
| GFEDv4.1s | - | 33.6 | 4.0 | 12.4 | 31.3 | 53.2 | 548.3 | 8519.7 | 16.7 | 2.2 | 11.7 |
| Xia et al, (2016) | 350.2 | 339.3 | 14.8 | 137.8 | - | - | 1989.9 | 49835.1 | 134.3 | 22.6 | - |

[1] FRP-based (WSE): the OBB emissions were estimated with FRP-based method, applying the same emission factors used in the bottom-up method. The emission factors were obtained by weighting emission factors in the bottom-up method with the masses of various crop types.

**Table 4. The uncertainties of OBB emissions in YRD indicated as 95% CIs and the top two parameters contributing most to emission uncertainties based on traditional bottom-up and FRP-based methods for 2012. The percentages in the parentheses indicate the contributions of the parameters to the variances of emissions.**

| | Traditional bottom-up method | | FRP-based method | |
|---|---|---|---|---|
| $PM_{10}$ | -56%, +70% | $PCRBF^{1}_{Anhui}$（42%）<br>$EF_{wheat}$ (41%) | -77%, +274% | EF (76%)<br>$AF^{2}$ (11%) |
| $PM_{2.5}$ | -56%, +70% | $PCRBF_{Anhui}$（43%）<br>$EF_{wheat}$ (41%) | -63%, +244% | EF (65%)<br>$NFP^{3}$ (16%) |
| EC | -50%, +54% | $PCRBF_{Anhui}$（69%）<br>$PCRBF_{Jiangsu}$（11%） | -78%, +281% | EF (75%)<br>NFP (11%) |
| OC | -54%, +73% | $PCRBF_{Anhui}$（42%）<br>$EF_{rice}$ (37%) | -78%, +276% | EF (75%)<br>NFP (11%) |
| $CH_4$ | -49%, +58% | $PCRBF_{Anhui}$（65%）<br>$PCRBF_{Jiangsu}$（11%） | -83%, +315% | EF (79%)<br>NFP (9%) |
| NMVOCs | -48%, +59% | $PCRBF_{Anhui}$（64%）<br>$PCRBF_{Jiangsu}$（10%） | -63%, +243% | EF (65%)<br>NFP (16%) |
| CO | -46%, +73% | $PCRBF_{Anhui}$（62%）<br>$PCRBF_{Jiangsu}$（10%） | -52%, +223% | EF (57%)<br>NFP (19%) |
| $CO_2$ | -48%, +60% | $PCRBF_{Anhui}$（69%）<br>$PCRBF_{Jiangsu}$（10%） | -21%, +164% | NFP (44%)<br>AF (42%) |
| $NO_X$ | -47%, +87% | $PCRBF_{Anhui}$（51%）<br>$EF_{wheat}$ (23%) | -82%, +303% | EF (78%)<br>NFP (10%) |
| $SO_2$ | -59%, +138% | $EF_{wheat}$ (35%)<br>$PCRBF_{Anhui}$（27%） | -78%, +279% | EF (74%)<br>NFP (12%) |
| $NH_3$ | -51%, +67% | $PCRBF_{Anhui}$（55%）<br>$EF_{wheat}$ (12%) | -82%, +302% | EF (79%)<br>NFP (10%) |

[1] PCRBF, the percentage of crop residues burned in the field (the subscript indicates province); [2] AF, the average FRE of fire pixels; [3] NFP, the number of fire pixels; [4] MCRBF, the mass of crop residues burned in the field.

1074 **Figure 1.**

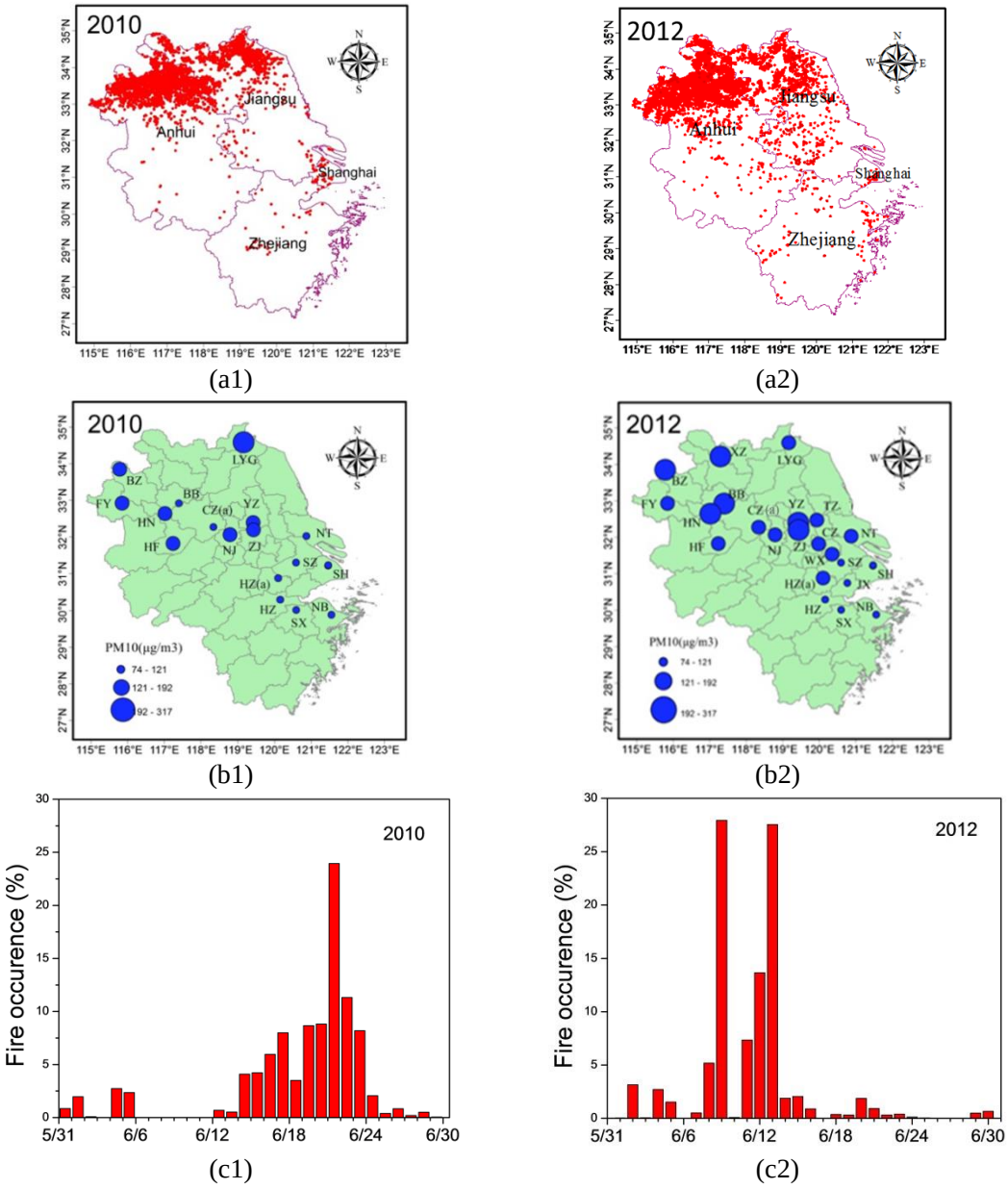


1075

1076 **Figure 2.**

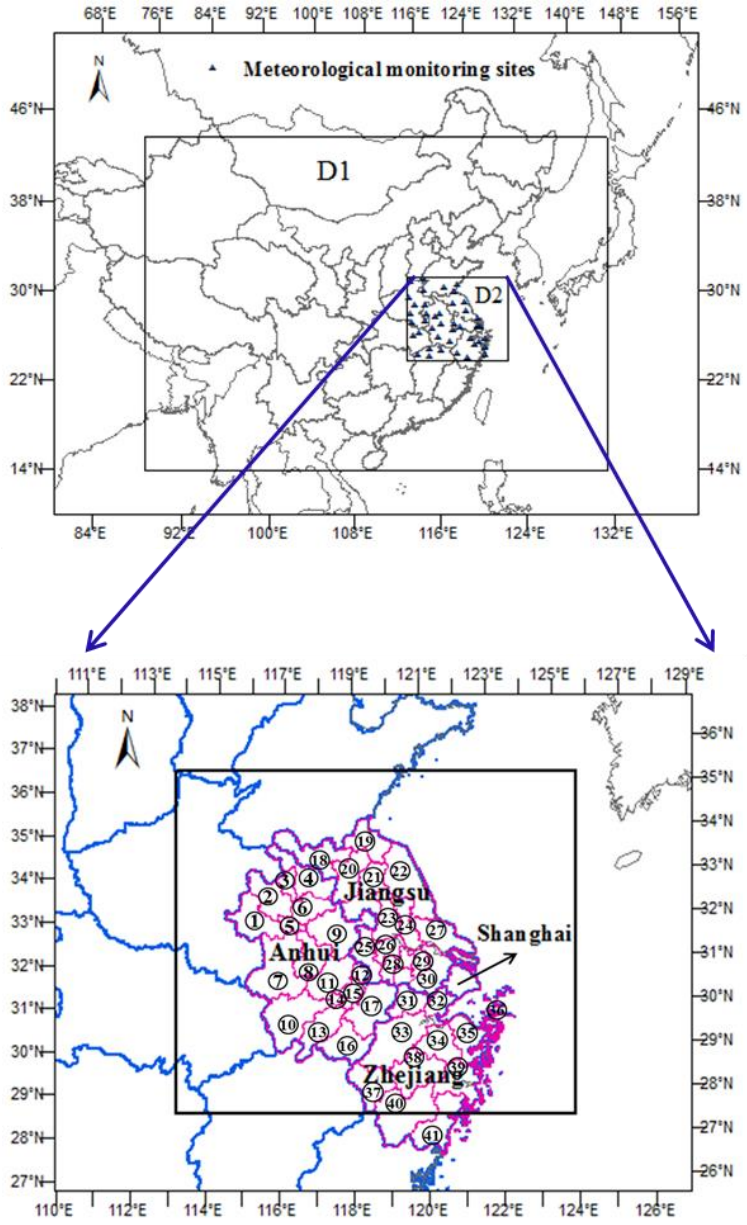


1077

1078

**Figure 3.**

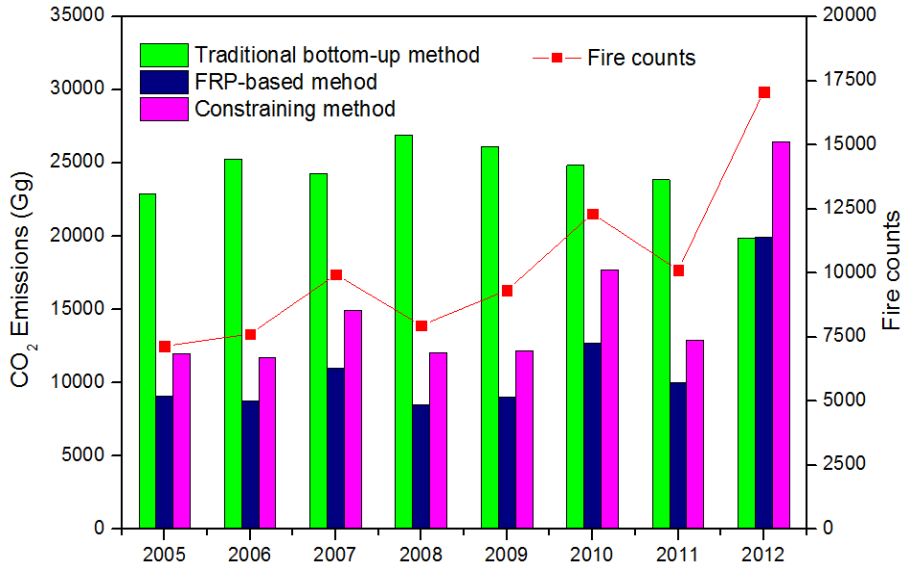
Traditional bottom-up method
FRP-based mehod
Constraining method
Fire counts
$CO_2$ Emissions (Gg)
Fire counts
35000
30000
25000
20000
15000
10000
5000
0
20000
17500
15000
12500
10000
7500
5000
2500
0
2005
2006
2007
2008
2009
2010
2011
2012

**Figure 4.**

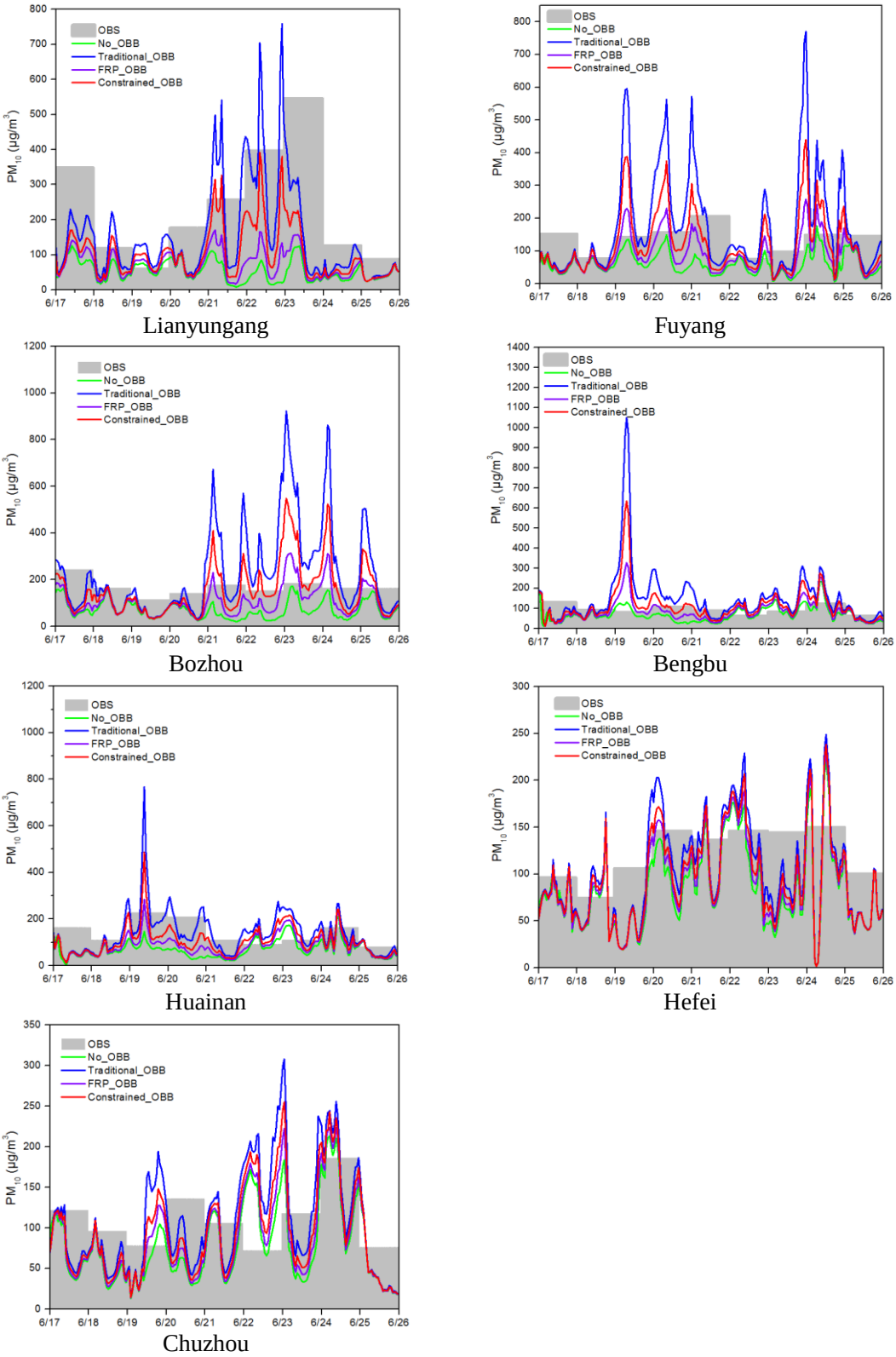
OBS
No_OBB
Traditional_OBB
FRP_OBB
Constrained_OBB
PM10 (μg/m3)
6/17
6/18
6/19
6/20
6/21
6/22
6/23
6/24
6/25
6/26
Lianyungang
Fuyang
Bozhou
Bengbu
Huainan
Hefei
Chuzhou

**Figure 5.**

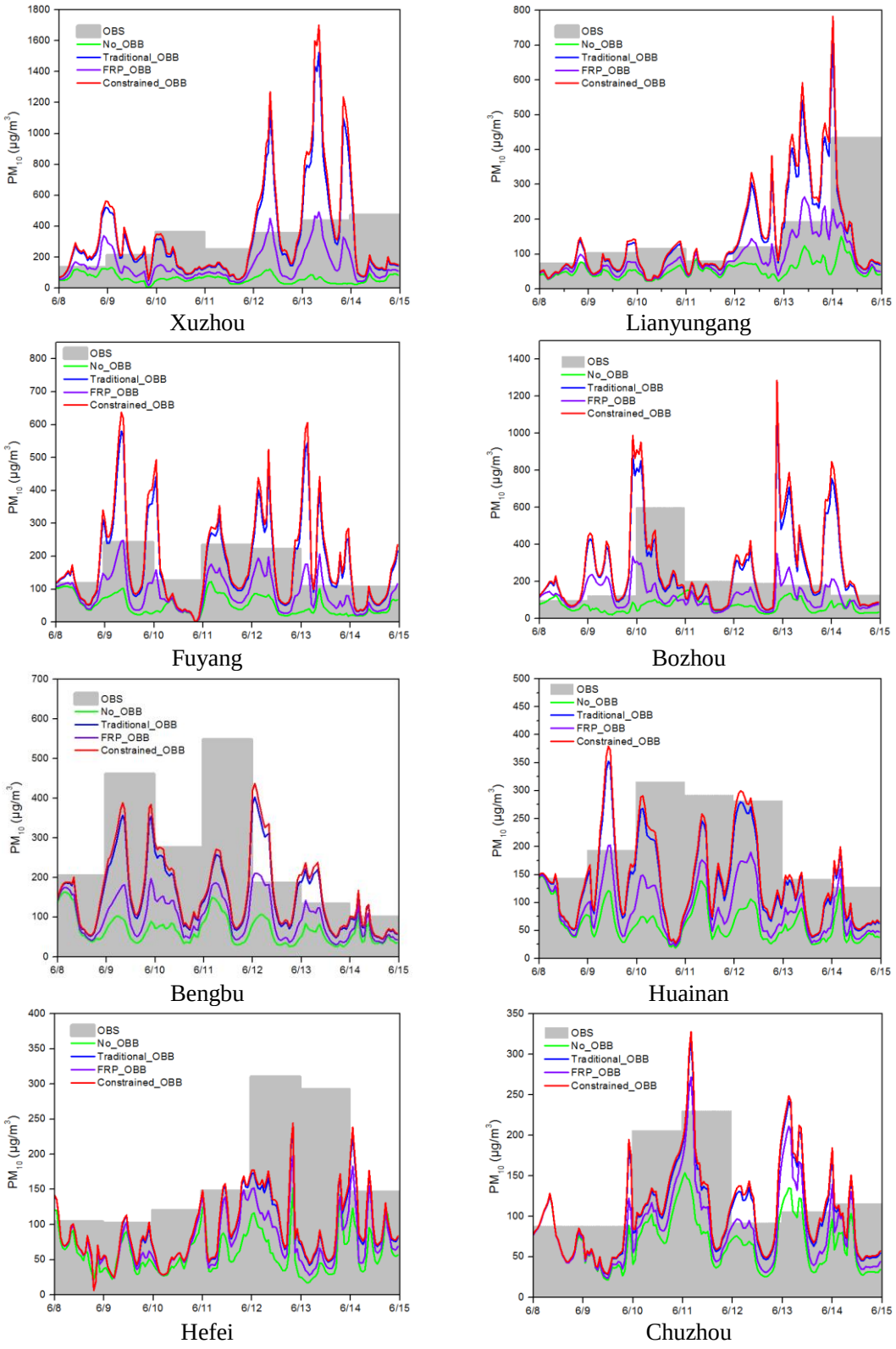
OBS
No_OBB
Traditional_OBB
FRP_OBB
Constrained_OBB
PM10 (μg/m3)
6/8
6/9
6/10
6/11
6/12
6/13
6/14
6/15
Xuzhou
Lianyungang
Fuyang
Bozhou
Bengbu
Huainan
Hefei
Chuzhou

**Figure 6.**

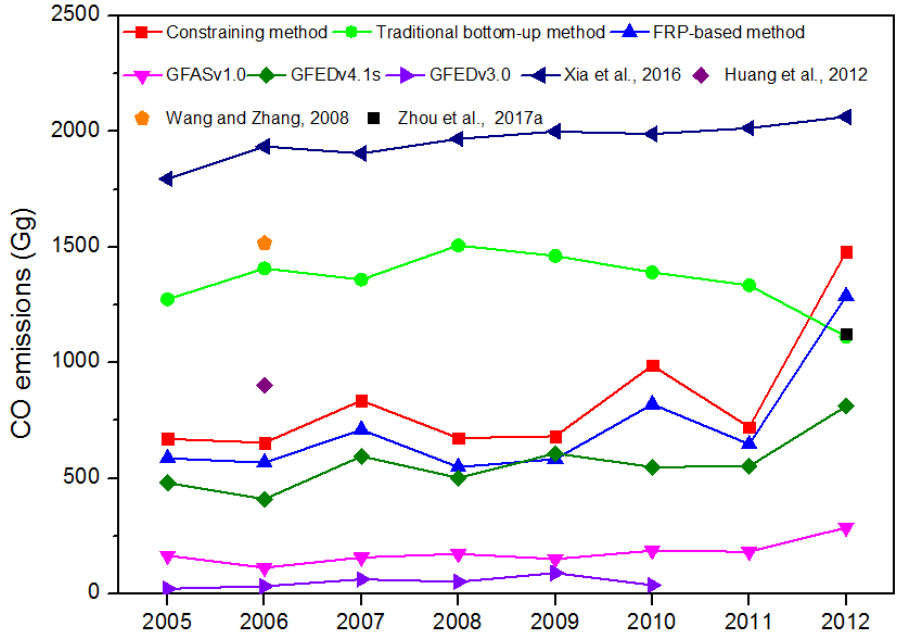
Constraining method
Traditional bottom-up method
FRP-based method
GFASv1.0
GFEDv4.1s
GFEDv3.0
Xia et al., 2016
Huang et al., 2012
Wang and Zhang, 2008
Zhou et al., 2017a
CO emissions (Gg)
2500
2000
1500
1000
500
0
2005
2006
2007
2008
2009
2010
2011
2012

**Figure 7.**

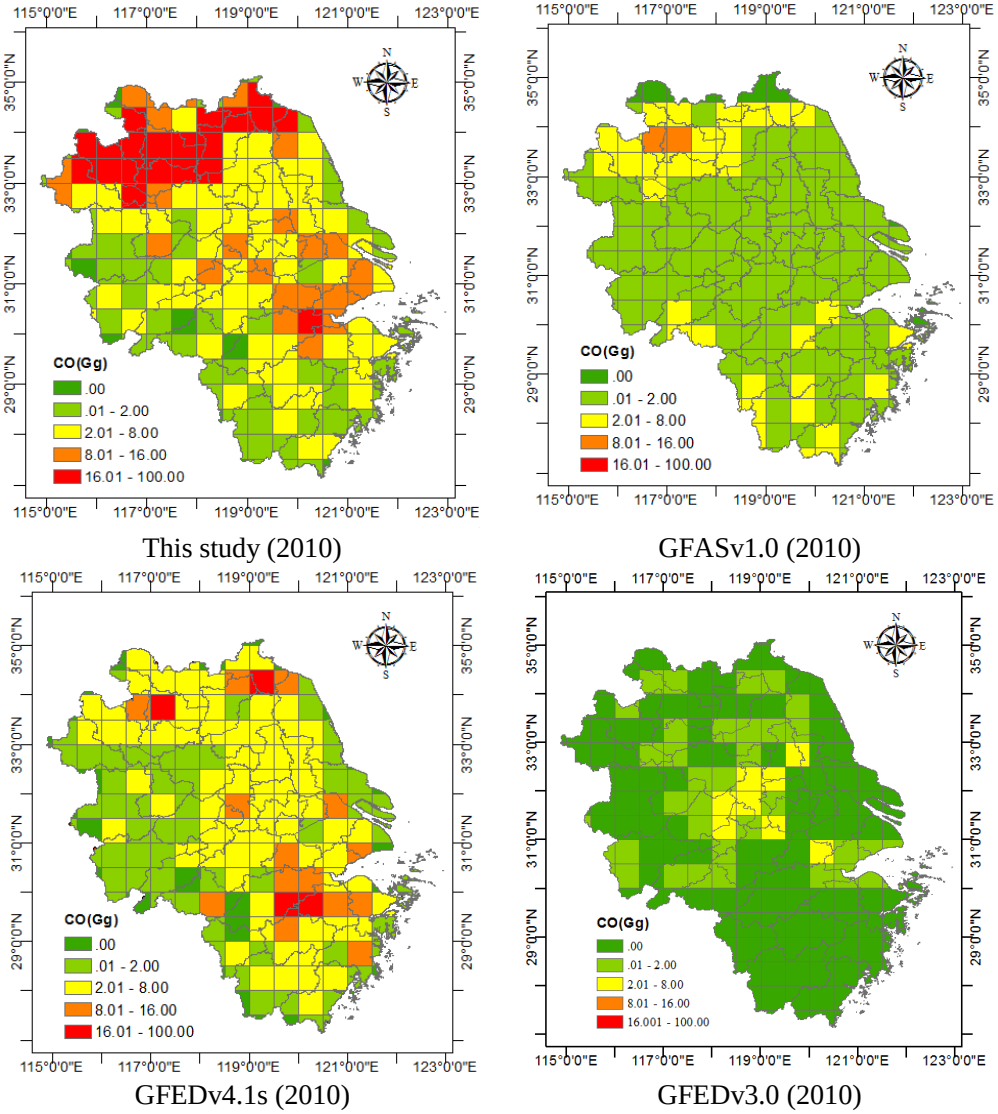
115°0'0"E
117°0'0"E
119°0'0"E
121°0'0"E
123°0'0"E
35°0'0"N
33°0'0"N
31°0'0"N
29°0'0"N
CO(Gg)
.00
.01 - 2.00
2.01 - 8.00
8.01 - 16.00
16.01 - 100.00
16.001 - 100.00
This study (2010)
GFASv1.0 (2010)
GFEDv4.1s (2010)
GFEDv3.0 (2010)

**Figure 8.**

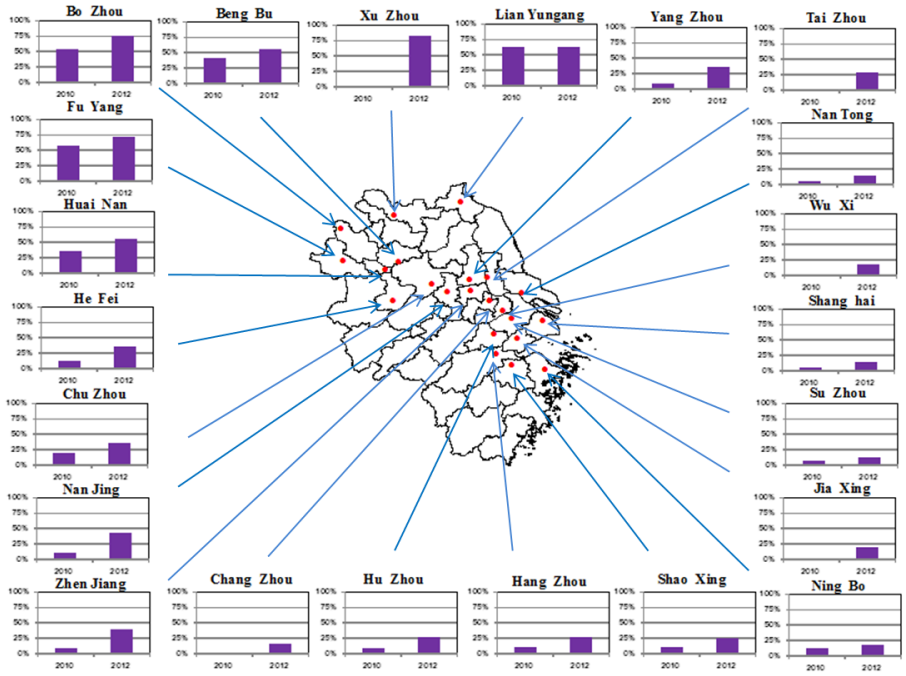
Bo Zhou
Beng Bu
Xu Zhou
Lian Yungang
Yang Zhou
Tai Zhou
Fu Yang
Nan Tong
Huai Nan
Wu Xi
He Fei
Shang hai
Chu Zhou
Su Zhou
Nan Jing
Jia Xing
Zhen Jiang
Chang Zhou
Hu Zhou
Hang Zhou
Shao Xing
Ning Bo
2010
2012

**Figure 9.**

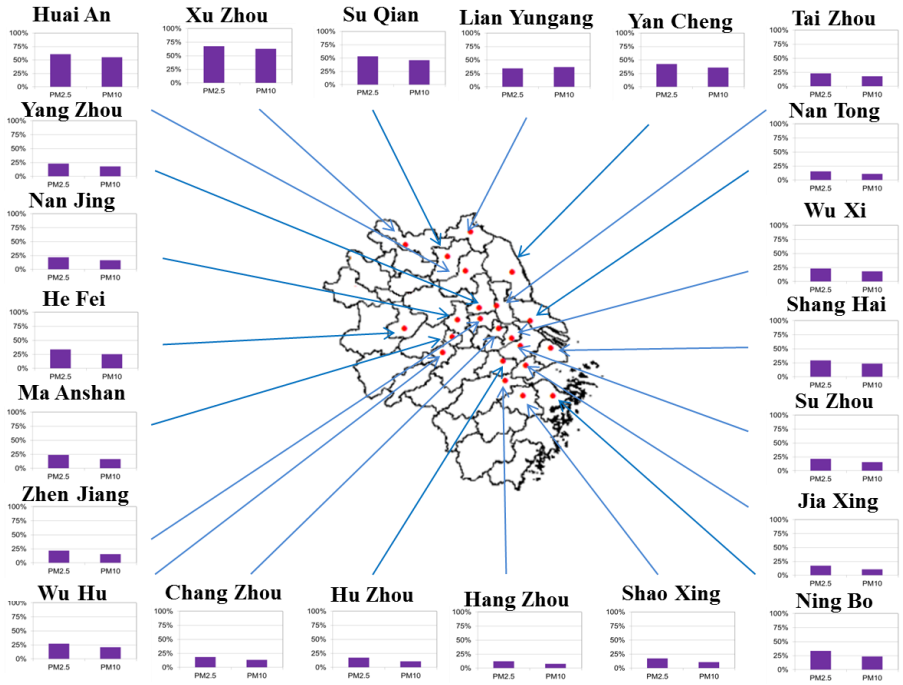
Huai An
Xu Zhou
Su Qian
Lian Yungang
Yan Cheng
Tai Zhou
Yang Zhou
Nan Tong
Nan Jing
Wu Xi
He Fei
Shang Hai
Ma Anshan
Su Zhou
Zhen Jiang
Jia Xing
Wu Hu
Chang Zhou
Hu Zhou
Hang Zhou
Shao Xing
Ning Bo
PM2.5
PM10

**Figure 10.**

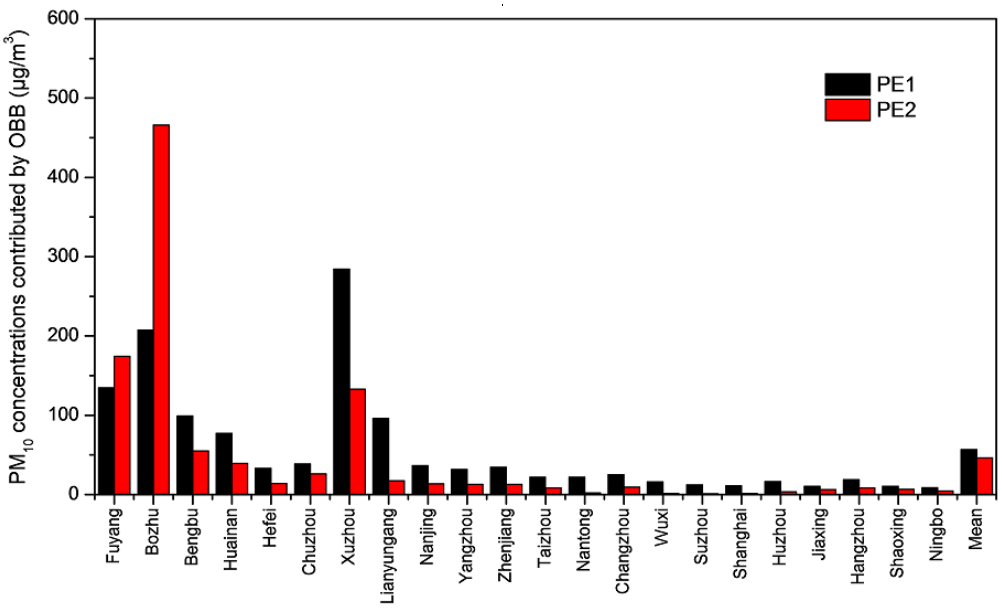
PM10 concentrations contributed by OBB (μg/m3)
600
500
400
300
200
100
0
PE1
PE2
Fuyang
Bozhu
Bengbu
Huainan
Hefei
Chuzhou
Xuzhou
Lianyungang
Nanjing
Yangzhou
Zhenjiang
Taizhou
Nantong
Changzhou
Wuxi
Suzhou
Shanghai
Huzhou
Jiaxing
Hangzhou
Shaoxing
Ningbo
Mean

**Figure 11.**

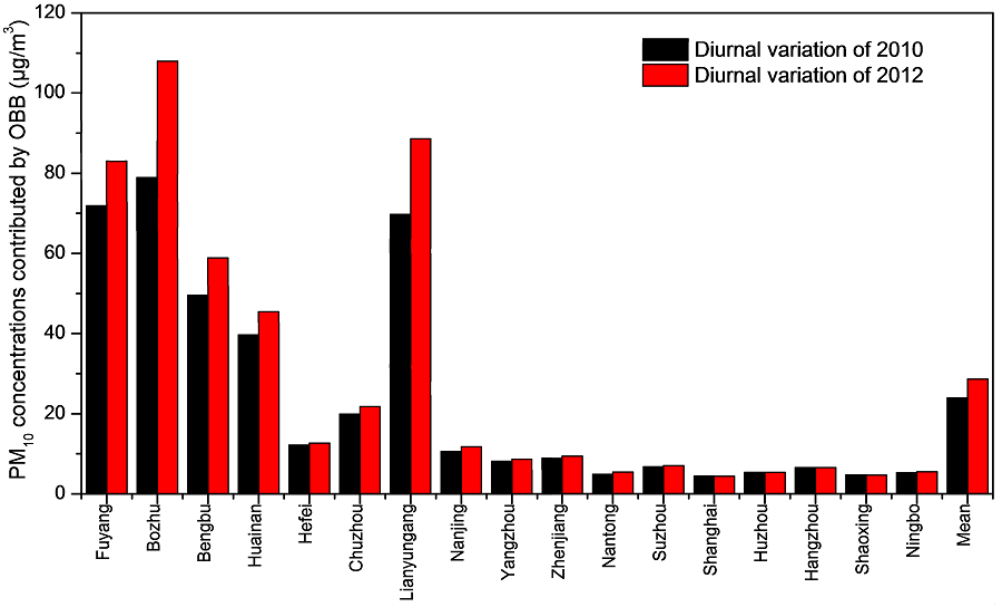
Diurnal variation of 2010
Diurnal variation of 2012
PM10 concentrations contributed by OBB (μg/m3)
0
20
40
60
80
100
120
Fuyang
Bozhu
Bengbu
Huainan
Hefei
Chuzhou
Lianyungang
Nanjing
Yangzhou
Zhenjiang
Nantong
Suzhou
Shanghai
Huzhou
Hangzhou
Shaoxing
Ningbo
Mean